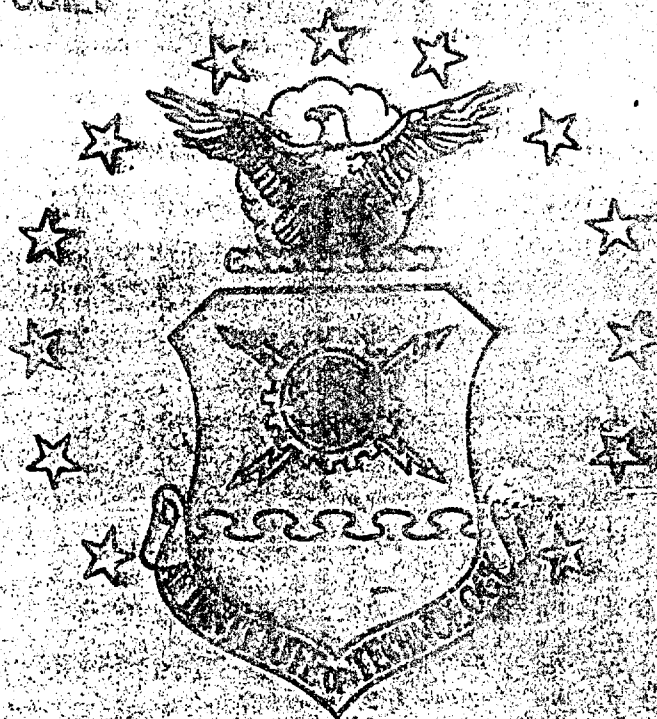AD-A229 867

AN EXPERIMENTAL STUDY OF A
STING-MOUNTED SINGLE-SLOT
CIRCULATION CONTROL WING

THESIS

Michael E. Pelletier, Captain, USAF

AFIT/GAF/ENY/90D-18

DEPARTMENT OF THE AIR FORCE

UNIVERSITY

AIR FORCE INSTITUTE OF TECHNOLOGY

AN EXPERIMENTAL STUDY OF A
STING-MOUNTED SINGLE-SLOT
CIRCULATION CONTROL WING

THESIS

Michael E. Pelletier, Captain, USAF

AFIT/GAE/ENY/90D-18

AFIT/GAE/ENY/90D-18

AN EXPERIMENTAL STUDY OF A

STING-MOUNTED SINGLE-SLOT

CIRCULATION CONTROL WING

THESIS

Presented to the Faculty of the School of Engineering

of the Air Force Institute of Technology

Air University

In Partial Fulfillment of the

Requirements for the Degree of

Master of Science in Aeronautical Engineering

Michael E. Pelletier, B.S.

Captain, USAF

December 1990

Acknowledgements

This thesis project is dedicated to the memory of Captain Wayne P. Wilsdon, fellow classmate and friend.

I have many people to thank for the help they gave me in completing this research effort. I would like to thank my advisor, Dr. Milton Franke, for his help. Mr. Dan Rioux from the AFIT aero labs provided technical support and invaluable aid in instrumentation and wind tunnel operation. I would also like to thank Mr. Dave Driscoll, Mr. Tim Hancock, and Mr. Jan LeValley from the AFIT model shop for taking my rough sketches and turning them into a first-rate model. Mr. Steve DeCook provided his expertise in writing and debugging data acquisition software; of this I am especially grateful. Finally, I would like to thank my best friend, my wife Michele, for her patience, encouragement, and support throughout this project. She provided the strength I needed when things were looking bleak (and they looked bleak often).

ii

Table of Contents

List of Figures

List of Tables

List of Symbols

A	area (ft^2)
AR	aspect ratio
AX	axial force (lb_f)
b	wing span (ft)
b_s	slot span
c	wing chord (ft)
CCW	circulation control wing
C_D	wing drag coefficient
C_{De}	wing equivalent drag coefficient
C_L	wing lift coefficient
C_{Mle}	wing moment coefficient about the leading edge
C_p	pressure coefficient
C_μ	momentum coefficient
C0	offset coefficient (lb_f/in^2)
C1	sensitivity coefficient [$lb_f/(in^2\text{-volt})$]
C2	nonlinearity coefficient [$lb_f/(in^2\text{-volt}^2)$]
ds	differential length
D	wing drag (lb_f)
D_e	equivalent drag
deg	degrees
h	slot height
in.	inches
ℓ	rolling moment
L	wing lift
LE	leading edge
$\dot{m}$	mass flow rate (slugs/sec)
M	Mach number
N1	normal force on element 1
N2	normal force on element 2
P	absolute pressure

psf	lb_f/ft^2
q	dynamic pressure (lb_f/ft^2)
r	Coanda surface radius
R	universal gas constant for air $R=1716\ ft^2/(sec^2\text{-}deg\ R)$
RE	Reynolds number based on wing chord
S'	total wing area affected by blowing (ft^2)
S	wing planform area (ft^2)
sec	second
T	temperature (deg Rankine)
t/c	thickness ratio
v	velocity (ft/sec)
$\vec{v}$	velocity tangent to airfoil surface (ft/sec)
V	volts
x/c	chordwise wing position
Y	compressibility factor
Y1	side force on element 1
Y2	side force on element 2
z	airfoil dimension measured normal to chord (ft)
α	angle of attack
Δ	incremental change
Γ	circulation (ft^2/sec)
ρ	air density $(slugs/ft^3)$
γ	ratio of specific heats for air $(\gamma=1.4)$

Subscripts

$(\ )_{atm}$ atmospheric conditions

$(\ )_j$ conditions in jet

$(\ )_1$ conditions upstream of venturi tube

$(\ )_2$ conditions at venturi tube throat

$(\ )_\infty$ free stream conditions

$(\ )_s$ static conditions

$(\ )_t$ plenum total conditions

Abstract

This wind tunnel study investigated the feasibility of using a sting and force balance to measure the aerodynamic forces and moments on a circulation control wing. A 20% thick, 8.5% camber, single blowing slot, rectangular wing was designed, built, and tested in the AFIT 5-ft wind tunnel. Lift and drag coefficients were referenced to the stability axis. The Reynolds number for all tests was 9×10^5; angle of attack was varied from -6 to +6 degrees. Trends in the data were similar to two dimensional data, with the exception of high drag coefficients with increased blowing. Results show it is feasible to test three dimensional wings using a sting and force balance if appropriate data corrections are applied.

xi

AN EXPERIMENTAL STUDY OF A STING-MOUNTED
SINGLE-SLOT CIRCULATION CONTROL WING

I. Introduction

Background

The development of V/STOL aircraft remains a challenge
that needs to be met. As aircraft cruise speeds become
increasingly faster, so do their takeoff and landing speeds.
The result of this is increased runway length needed for
safe operation, as well as increased wear and tear on
landing gear components. For civilian applications V/STOL
aircraft permit shorter runways and reduced noise footprints
due to steeper climbout angles. Military aircraft benefit
from V/STOL technology by being able to operate off runways
made shorter through design, necessity, or enemy munitions.
Steeper climb and descent angles of tactical airlift
aircraft also reduce the exposure time to small arms fire
from the ground.

Many techniques exist for obtaining the high lift
coefficients required by V/STOL aircraft. These include
tilt wings, tilt rotors, vectored thrust, and blown flaps.
One disadvantage of these systems is the requirement of
complex mechanical devices for their operation. One fairly
simple technique that exists for increasing lift is
circulation control. Circulation control wings use the

1

Coanda effect to increase the circulation around a wing and hence the lift. This effect is due to the familiar Kutta-Joukowski theorem, which states the lift is proportional to the circulation (Γ) around the airfoil. This equation takes the form

$$L = \rho v \Gamma \qquad (1)$$

with

$$\Gamma = \oint_c \vec{v} \cdot d\vec{s} \qquad (2)$$

where $\vec{v} \cdot d\vec{s}$ is the dot product of the velocity vector and a differential length around the closed curve c.

The trailing edge of a circulation control airfoil is characteristically blunt, typically circular. The Coanda effect describes the adherence of a low pressure sheet of air to the curved trailing edge of an airfoil. This occurs due to a balance between the centrifugal force in the jet and the reduced pressure on the surface due to the jet velocity. For low blowing rates the jet sheet serves as a boundary layer control, reenergizing the boundary layer and delaying separation. At higher blowing rates the forward and aft stagnation points begin to move towards the bottom of the airfoil, increasing the circulation and hence the lift.

Previous Research

Much research has been done in the area of circulation control airfoils. Kind and Maull (1:170-182), in their investigation of a low speed circulation control airfoil, obtained lift coefficients greater than 3.0. Williams and Howe (2:9) were able to obtain a lift coefficient of 6.30 using a 20 percent thick, 5 percent cambered airfoil. Later, Englar (References 3 and 4) was able to obtain lift coefficients as high as 6.5 at low blowing rates. In addition to wind tunnel studies, flight tests on aircraft have been made using circulation control wings (CCW). Both Loth (5) and Grumman Aerospace Corporation (6) modified and successfully flew demonstrator CCW aircraft.

Considerable research has also taken place at AFIT. A Master's thesis by Harvell (7) found under some circumstances for a given blowing rate two slots are better than one. Splitter plate effects on circulation control airfoils have also been investigated (8).

Present Study

Although there is a great deal of literature on two dimensional circulation control airfoils, little research has been done using three dimensional models. Recently, Trainor (9) tested a three dimensional model in the AFIT wind tunnel. His results show that using a sting and force balance for data acquisition is feasible and can give good results if adequate corrections are made to the data.

3

Trainor also found that interference from the sting and air supply hoses was disrupting the flow at the trailing edge and preventing strong Coanda turning. His recommendations for model changes were incorporated into the model used in this study.

For the study presented here, a single blowing slot, rectangular wing was designed, built, and tested in the AFIT 5-ft wind tunnel at a Reynolds number of 9×10^5. Force data were collected using a sting and 0.5-in. force balance. Pressure data were taken and used to correlate force balance findings and determine Coanda turning effectiveness.

II. Test Item Description and Instrumentation

Wing Model

The model constructed for this test was a 20-percent thick, 8.5-percent cambered, rectangular wing with a single trailing edge blowing slot. Photos of the model installed in the wind tunnel are shown in Figure 1. The elliptic airfoil had the same basic cross section as that tested by Harvell (7) and Trainor (9). Figures 2 and 3 show the wing cross section and provide details on the geometry of the model. The primary structural material was 3/32-in. aluminum, with a 0.045-in. fiberglass skin providing the upper airfoil surface. Since the sting entered the model through the trailing edge, the trailing edge slot was divided into a right and left 9.90625-in. slot fed by plenum chambers within the model.

Trainor's model was used as a guideline for sizing the planform. The 0.5-in. force balance used in the wind tunnel had limits of 200 lb_f normal and 50 lb_f axial force. Tests were planned using a Reynolds number approaching 10^6. The maximum dynamic pressure in the tunnel was calculated to be no greater than 42 psf. A C_{Lmax} of 3.0 was assumed based on Harvell's work (it turned out this was being overly optimistic). From these considerations the maximum model planform area was calculated. Assuming a chord (c) of 10 inches, the model span was then computed as 23.25 inches. This yielded a total blowing slot length of 19.8125 inches

5

Model Mounted in Tunnel Looking Downstream
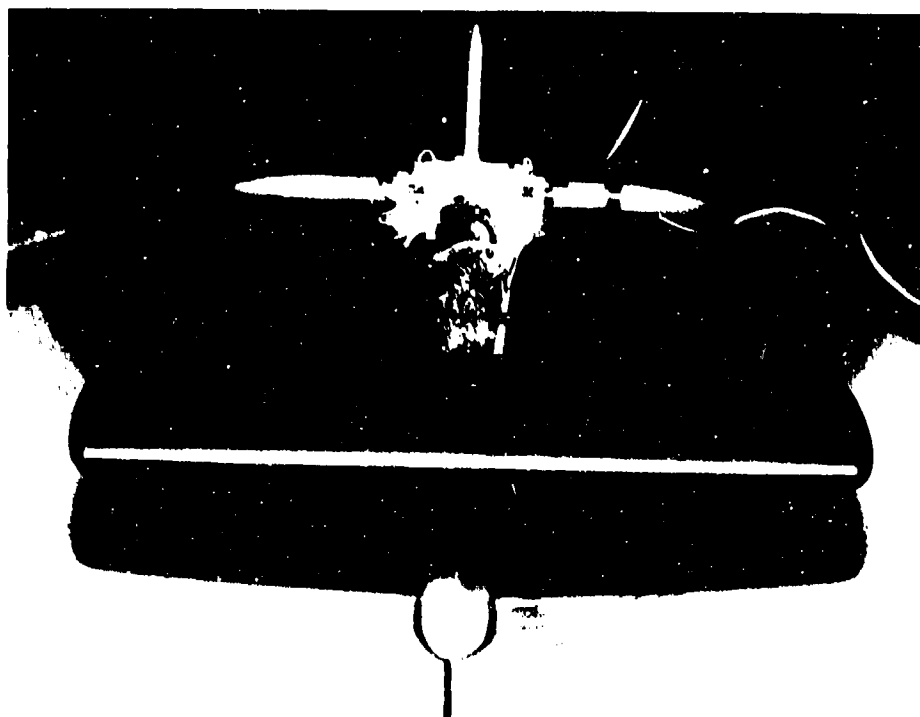
Model Mounted in Tunnel Looking Upstream
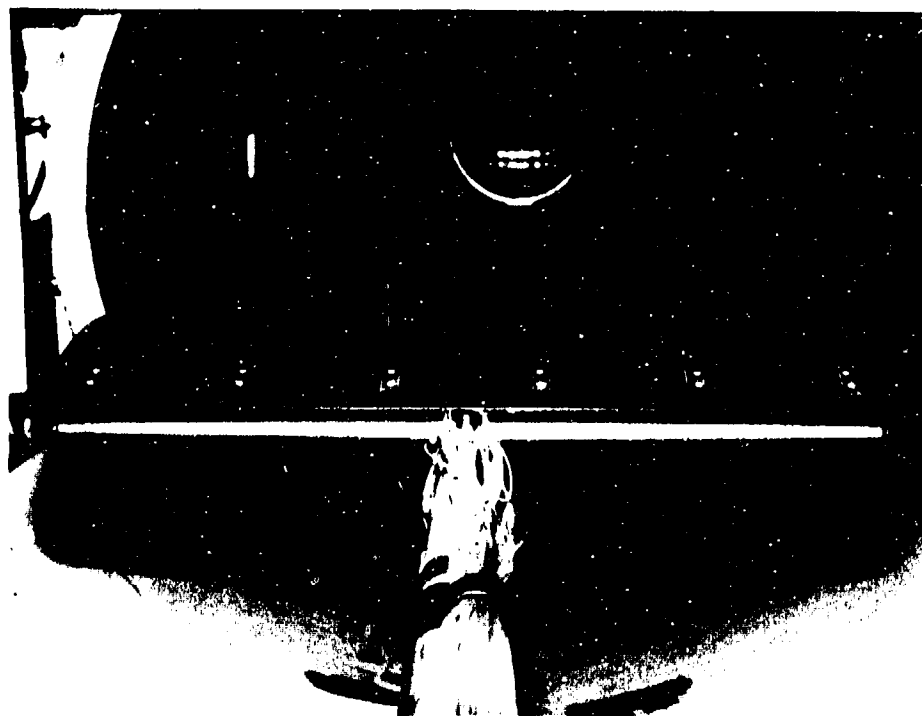
Figure 1.   Model Mounted in Wind Tunnel

6
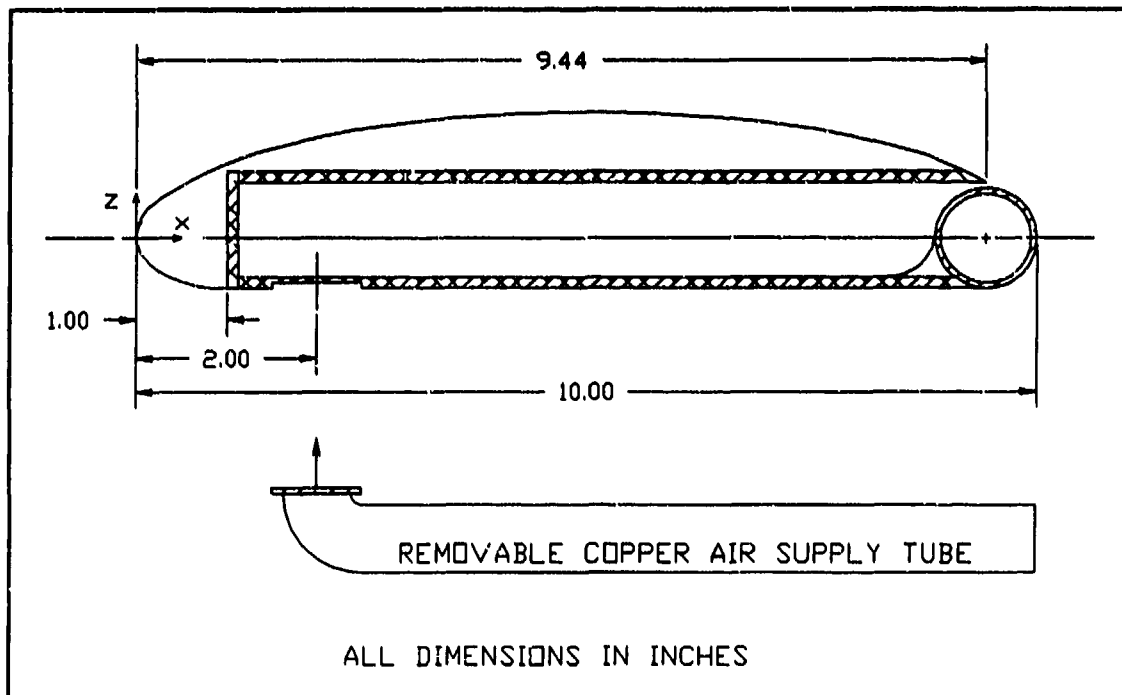
Figure 2. Elliptical Airfoil Cross Section

Upper Surface:

$$Z_u = 0.28\sqrt{5^2-(5-X)^2} \qquad 0 \le X \le 9.44$$

Lower Surface:

$$Z_l = -0.56\sqrt{1^2-(1-X)^2} \qquad 0 \le X \le 1$$
$$Z_l = -0.56 \qquad\qquad\qquad 1 < X \le 9.44$$

Coanda Surface:

$$Z_{cyl} = \pm\sqrt{0.56^2-(X-9.44)^2} \quad 9.44 < X \le 10$$
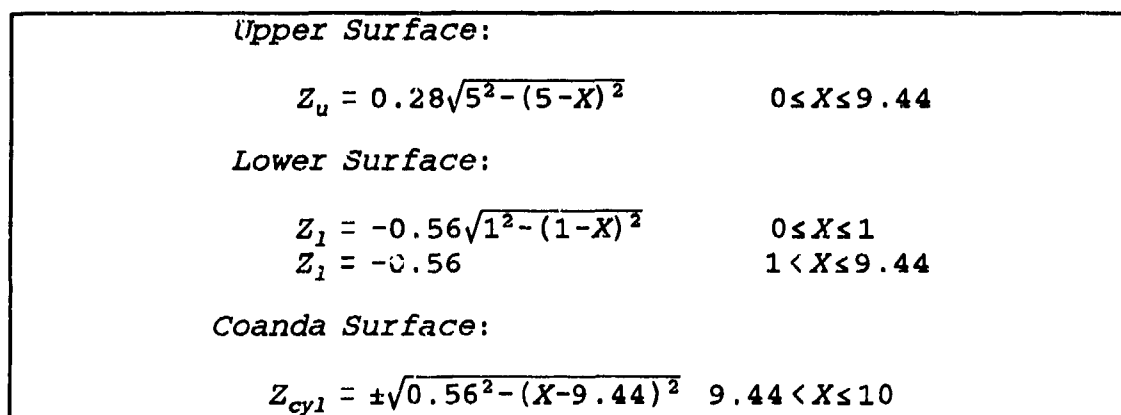
Figure 3. Elliptical Airfoil Geometry

and provided a 1.0625-in. region at midspan to mount the sting and run desired pressure tap hoses. One-inch elliptical fiberglass wing tips (visible in Figure 1) brought the total span to 23.25 inches; the model aspect ratio was 2.235. The maximum chord/tunnel height ratio of 0.25 proposed by Wood (10:4) for circulation control wings was met by the model. However, the low aspect ratio fell short of Wood's recommended aspect ratio of 4.0. It was felt the low aspect ratio of the model contributed strongly to reduced performance of the wing--lift coefficients were much less than expected. Wood's explanation for this is that interference caused by the tunnel walls produces unknown downwash effects.

Although a force balance was used to determine force coefficients for the model, pressure data were also desired. Following Pope and Rae (11:229) a total of 58 pressure taps were placed at three spanwise locations (Table 1). A single total pressure tap was located inside both the right and left plenum chambers near the Coanda surface to determine plenum stagnation pressure.

The trailing edge Coanda surface and blowing slot were designed following Englar's work (4:3). A trailing edge radius-to-chord ratio (r/c) was desired between 0.02 and 0.05 to provide effective Coanda turning. In addition it was desired to maintain a slot height-to-trailing edge radius (h/r) $\leq$ 0.05. Combining the two ratios yielded a

8

Table 1.   Pressure Tap Locations

Each position had both an upper surface tap and a
corresponding lower surface tap.

left side 6-in. from wing tip	left side 10-in. from wing tip	right side 6-in. from wing tip
x/c	x/c	x/c
0.00	0.00	0.00
0.025		
0.050		
0.10	0.10	0.10
0.20		
0.30	0.30	0.30
0.40		
0.50		
0.60	0.60	0.60
0.70		
0.80		
0.90	0.90	0.90
0.94	0.94	0.94
0.97		
0.99		
1.00		

desired slot height-to-chord ratio of $0.0005 \leq h/c \leq 0.0025$. With a slot height of 0.015 inches and a trailing edge radius of 0.56 inches, $h/c = .0015$, $h/r = .0268$, and $r/c = .056$. Although r/c was slightly higher than recommended by Englar (4), this was deemed acceptable in light of the other parameters being within limits. Six slot height adjustment screws were provided to maintain the slot height at the desired value; these were adjusted to maintain an even velocity profile across the slot. To encourage the flow to exit tangentially to the trailing edge the slot was undercut slightly following Englar's recommendation (4:5). Details of the trailing edge and slot design are shown in Figure 4.

The model was built around a single plenum chamber divided into right and left plenum chambers by a sting mounting block located at midspan (Figure 5). The large plenum chamber was made of 3/32-in. thick aluminum plate bolted together and sealed with epoxy. Plenum chambers were supplied with blowing air via a single removable 3/4-in. inside diameter copper tube entering the sting mounting block through the bottom of the model. A fiberglass fairing was mounted on the bottom of the model and covered the copper air supply tube as it ran along the bottom of the model (Figure 1). From the sting mounting block the air was routed to a slotted air distribution tube running spanwise along the front of each plenum chamber. To provide flow straightening with minimum pressure loss 1/4-in. honeycomb

10

FIBERGLASS SKIN ⌐
SLOT ADJUSTMENT SCREW
UNDERCUT IN SLOT
h
COANDA SURFACE
r=0.56"
SLOT ADJUSTMENT POST
▨ ALUMINUM   ▨ COPPER
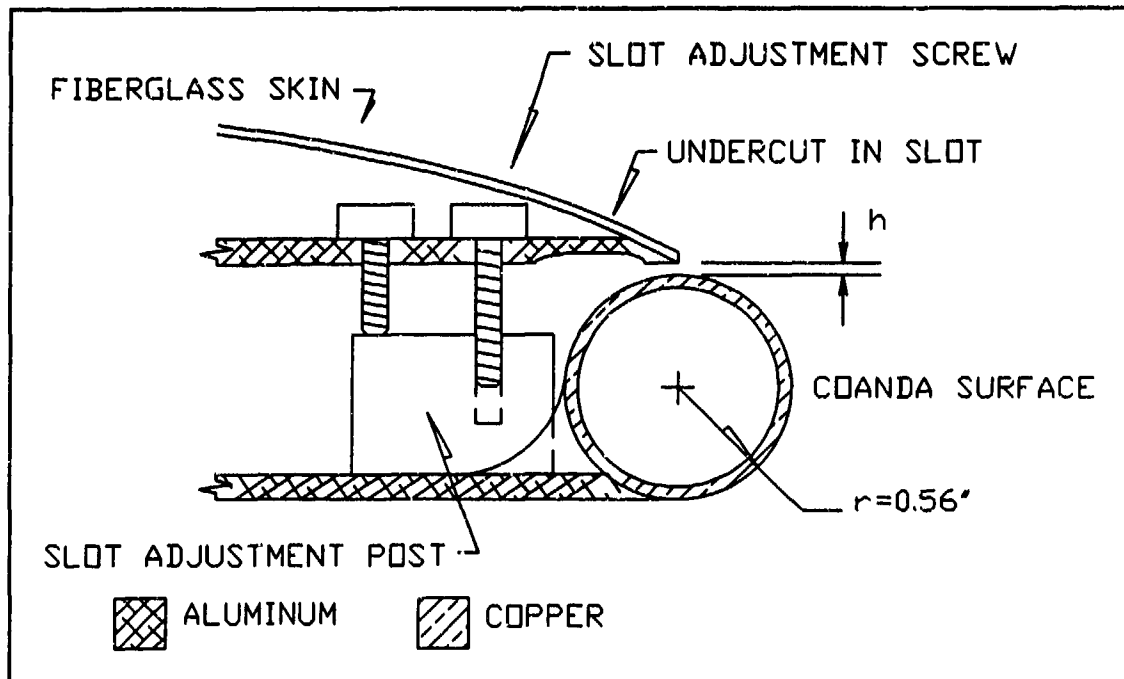
Figure 4. Trailing Edge and Slot Detail

STING MOUNTING BLOCK   AIR DISTRIBUTION TUBES
0.625
5.28
4.155
9.00
HONEYCOMB   HONEYCOMB
COANDA SURFACE   COANDA SURFACE
1.12
1.0625
10.00
21.25
SLOT ADJUSTMENT POST (TYP)
ALL DIMENSIONS IN INCHES
▨ 3/32" ALUMINUM
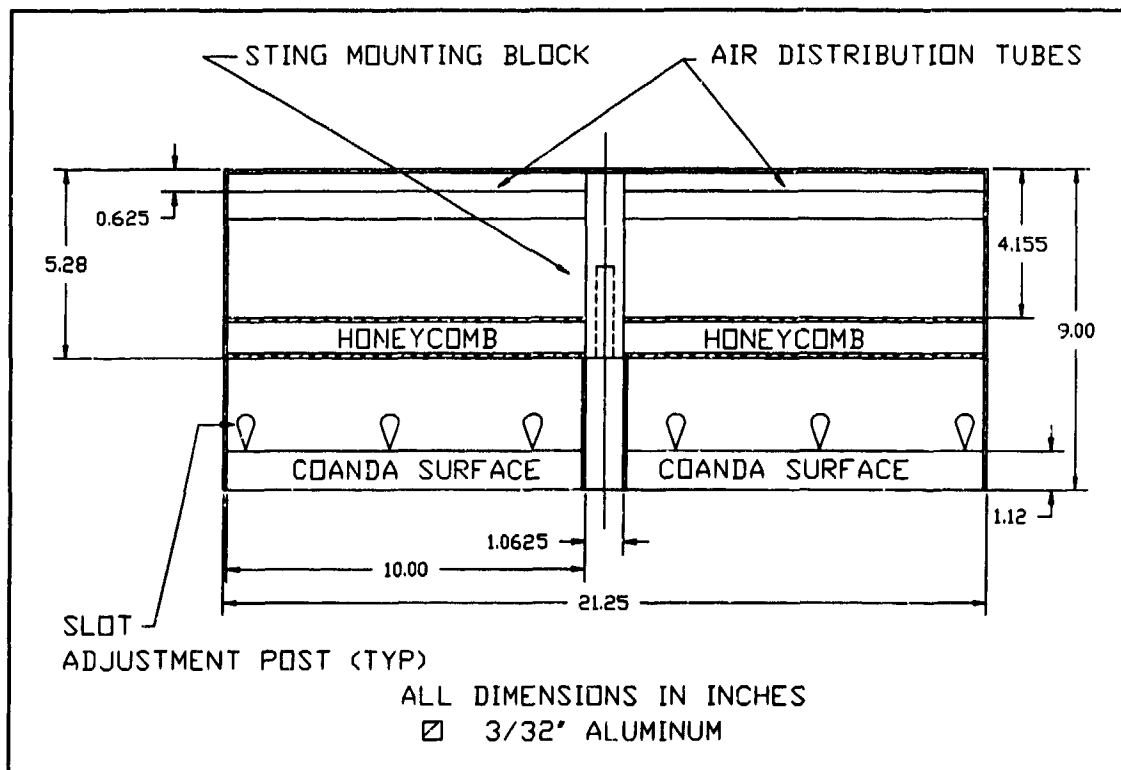
Figure 5. Plenum Chamber Plan View

11

screens one inch wide were installed spanwise near the mid-chord position. A chromel-alumel thermocouple installed in the left plenum chamber measured plenum total temperature. The Coanda surface was made of hollow copper tubing turned down on a lathe to a 0.56-in. radius. All pressure tap lines were routed along the floor or on top of the plenum chambers to exit within the 1.0625-in. gap at the trailing edge between the blowing slots.

Blowing Air Supply System

The blowing air supply system is shown in Figure 6. Shop air at approximately 100 psia entered a cyclone separator for filtration and removal of moisture. From there the air was routed to a regulator valve, used to maintain the plenum pressure. A chromel-alumel thermocouple installed in the supply line measured the flow temperature. The air then flowed through a shutoff valve to a calibrated 0.5-in. diameter venturi tube flow meter. Two 50-in. U-tube manometers measured the pressure upstream of the venturi throat and at the throat using flange taps. Both manometers were referenced to atmospheric pressure and produced gauge pressure readings. A 1-in. o.d., 3/4-in. i.d. vinyl hose was routed from the venturi tube to the model. The hose entered the tunnel downstream of the model and was then routed along the sting. A hose clamp secured the vinyl hose to the copper air supply tube on the model.
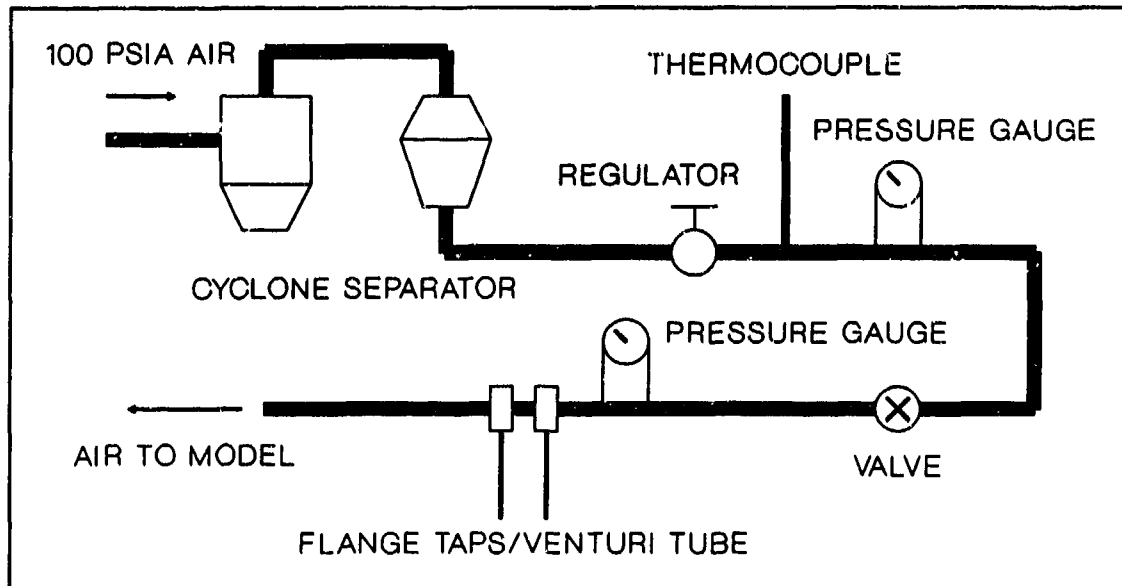
Figure 6. Blowing Air Supply

AFIT 5-ft Wind Tunnel

The AFIT 5-ft wind tunnel at Wright-Patterson Air Force Base was used to perform all tests. This tunnel is an open-circuit, closed-test section, continuous flow tunnel. It has a contraction ratio of 3.7 to 1 and a 5-ft diameter test section. Tunnel velocities as high as 200 mph are provided by two counterrotating 12-ft fans. Total pressure for the tunnel is assumed to be atmospheric, while static pressure is taken off a row of eight static ports located 2.5-feet from the tunnel mouth. "Tunnel q", or dynamic pressure, is measured as the difference between the total pressure and the tunnel static pressure and is displayed on a micromanometer in inches of water (in. H_2O). Tunnel q was calculated each time for the given static conditions to provide the required Reynolds number and maintained

13

throughout the test. Tunnel q calculations were made using a MathCAD* program. The turbulence factor for the tunnel is 1.5, (11:147) which accounts for turbulence produced in the tunnel by the guide vanes, the propellers, and tunnel wall vibration. To compare test results obtained in other tunnels or flight tests the effective Reynolds number (defined as this test's Reynolds number times the turbulence factor) should be used.

Force Balance and Data Acquisition System

The 0.5-in., six-component force balance (model designation: Mark V) used in the AFIT 5-ft wind tunnel is made by the Able Corporation. The sign convention for all loadings is shown in Figure 7. Normal force limits for the N1 and N2 strain gages are 100 lb_f each, for a total normal force limit of 200 lb_f. Side force limits for the Y1 and Y2 gages are 50 lb_f each, the axial force limit for the AX gage is 50 lb_f, and the rolling moment limit is 40 in.-lb_f. Excitation voltage for all strain gages is supplied by a regulated d.c. power supply.

Prior to testing, several calibrations were necessary for the sting and force balance. First, check loads were required to ensure the accuracy of the existing balance calibration file. A series of ten-pound weights were hung from the force balance without the model installed and force measurements made. Each gage was loaded through a calibration body mounted on the balance in both the positive

14

ARROW INDICATES POSITIVE LOAD
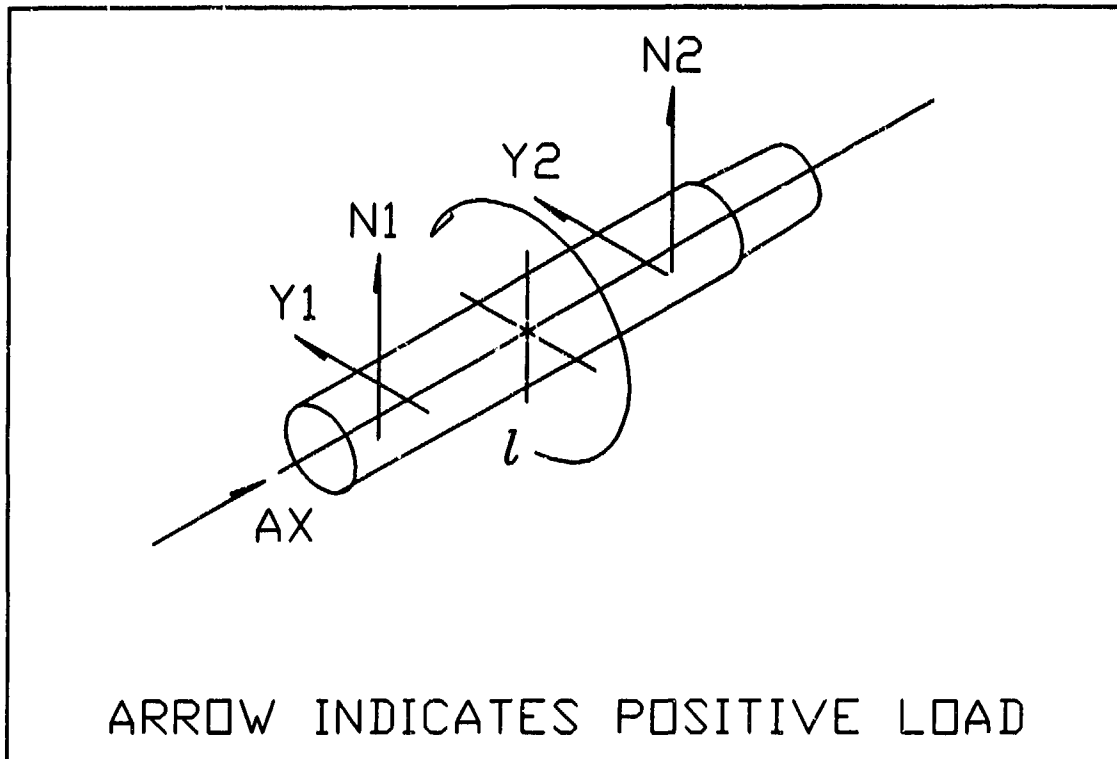
Figure 7. Force Conventions for Able Corp. Mark V
Six-Component Force Balance

and negative directions, with the exception of the axial force gage, which was only loaded in the positive direction. Maximum load in the N1, N2, Y1, and Y2 directions (positive and negative) was 60 lb_f. Maximum load in the AX direction was 50 lb_f.

The data acquisition system was used to record the voltage output from each gage for each applied load. This data was reduced using software within the data acquisition system into forces, which were compared to the known applied loads. All forces were found to be within two percent, which verified the accuracy of the force balance calibration

15

data. Similar check loads were made at the completion of tests with the model installed on the sting. Two pound weights were applied to the top of the model and force data taken until a total of 10 pounds was applied to the model. Comparing applied loads with reduced force data again showed accuracy within two percent. There did not appear to be any interference between the model and the force balance. Higher loads were not applied to avoid crushing the fiberglass upper surface of the model. Loadings in other than the negative N1 and N2 directions were not accomplished due to a lack of equipment capable of providing the appropriate loads.

A second type of required calibration was sting angle due to bend. This was an angle-to-volts curve automatically generated during force balance calibration. This calibration curve was used in the data reduction routines to compensate for the sting bending when a load was applied. The results of this curve showed up in the reduced data for each run. Although the model was set at a given angle of attack for each test, due to forces generated during the run the model would actually change its own angle of attack. This change in α was on the order of two degrees for each run. Compensating for the change in α will be explained further in the section on data reduction.

The third calibration required was an angle-to-volts calibration. The model was mounted on the sting and placed

at known angles of attack using an inclinometer. The voltage output from a position potentiometer connected to the sting was manually recorded. The data acquisition software reduced this data into an angle-to-volts curve used in data reduction. This curve was also used to set the model at the required angle of attack for each run.

The data acquisition system used in the tunnel affords the user complete control over data acquisition and reduction, as well as displaying final output. The heart of the system is a Zenith Z-248 computer with an 80386 central processing unit. Other hardware includes a Hewlett-Packard HP 3852A Digital Acquisition and Control Unit (DACU) and a National Instruments IEEE-488 General Purpose Interface Bus (GPIB). There is also a Model 780B/T Pressure Measurement System (PMS) made by Pressure Systems Incorporated for pressure data collection; this will be discussed later. Figure 8 is a diagram of the data acquisition system hardware.

Software in the data acquisition library allows complete control over all force balance calibrations, model and tunnel configuration data, force balance data collection, and reduction routines. All software routines are described in Reference 12. The system has the capability to run external programs written by the user; one such program was used to control the 780B/T PMS. Other data collected by the data acquisition system includes
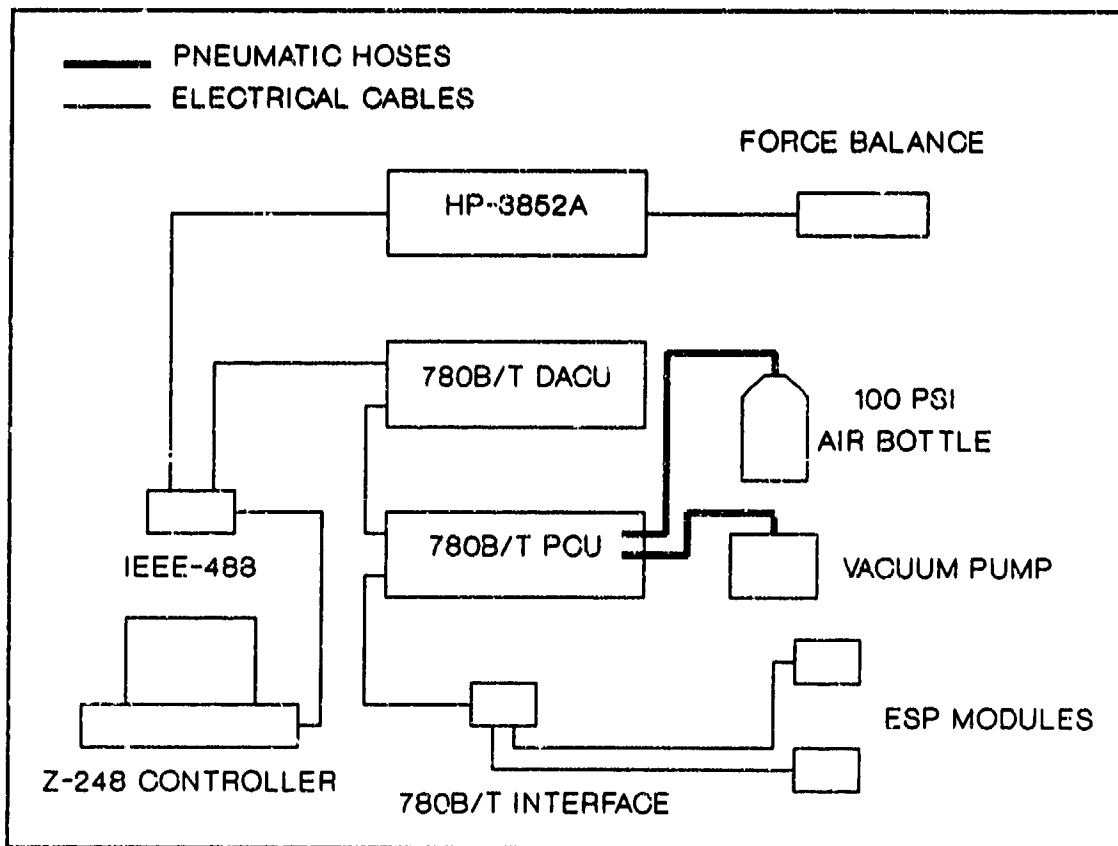
Figure 8. Data Acquisition System Hardware

atmospheric temperature, tunnel static pressure, and total pressure at the base of the sting. Atmospheric pressure (assumed to be tunnel total pressure) is entered manually and is required for calculating tunnel q using the incompressible Bernoulli equation.

Pressure Measuring System

Pressure data for the model were acquired using a Model 780B/T Pressure Measurement System. A complete description of this system is given in Reference 13. The system consists of a Data Acquisition and Control Unit (DACU), a Pressure Calibrate Unit (PCU), an interface unit, and

18

Electronically Scanning Pressure (ESP) modules. Commands can be entered from the front face of the 780B/T DACU or through an IEEE-488 bus and a system controller, such as the Z-248 computer. The system provides for up to 20000 samples per second. It also provides for rapid on-line calibration to ensure accuracy.

The PCU contains pneumatic valving and three highly accurate quartz pressure transducers used to calibrate the ESP modules. A 100 psia air bottle supplied pressure to the PCU for calibrating the ESP modules and controlling pneumatic run/calibrate valves within each module. Three separate pressure ranges are available to the user. Nine regulators within the PCU allow the user to set a low, medium, and high calibration pressure for each pressure range. The user can also supply external calibration pressures to the PCU, including subatmospheric pressures through a vacuum pump connection.

The ESP modules contain 32 ports, with one pressure transducer per port. The modules measure a differential pressure across each port (psid). For this test each module was referenced to atmospheric pressure. Two modules were mounted to the sting with their pressure ports connected to the model pressure taps using conventional pressure tubing.

Pressure data were collected simultaneously with force balance data through the data acquisition system. Prior to each run, the ESP modules were calibrated. Upon commands

19

from the system controller the PCU sent 100 psi air to each
module to trip a run/calibrate valve to the calibrate
position. Preset calibration pressures (set via the PCU
regulators) were then sent to each module and its
corresponding quartz pressure transducer within the PCU.
The calibration data is reduced by the 780B/T DACU into a
characteristic equation of the form

$$P = C0 + C1(V) + C2(V^2) \tag{3}$$

where P is the unknown pressure. The coefficients C0, C1,
and C2 are stored for each port in the 780B/T DACU and used
to calculate pressures taken from the model. Two ESP
modules were used for this test, a ±5 psid module used to
measure pressures on the top surface of the model (suction
side) and a ±45 psid module used for the lower surface
(pressure side), leading edge, and plenum chamber pressures.

III. Experimental Procedure

Model Checkout

Before testing of the model began several checkout procedures were completed. The air supply hose was connected to the model and the model plenum chambers were pressurized. No leaks were found in the model itself, although several small leaks were found in the fitting used to secure the copper air supply tube to the model. Application of silicone room-temperature vulcanizing (RTV) sealer to the fitting and then reinstalling it and allowing the RTV to cure eliminated any leaks. The slot height of the model was set at 0.015-in. using a feeler gauge. A pitot tube was mounted on a traversing rod and adjusted to measure the jet velocity at the slot. Assuming isentropic expansion through the slot allows the use of the relations

$$\frac{P_t}{P_j} = \left(1 + \frac{\gamma-1}{\gamma} M_j^2\right)^{\frac{\gamma}{\gamma-1}} \qquad (4)$$

and

$$\frac{T_t}{T_j} = \left(1 + \frac{\gamma-1}{2} M_j^2\right) \qquad (5)$$

with the Mach number defined as

$$M_j = \sqrt{\gamma R T_j} \qquad (6)$$

Using algebra and the above relations the jet velocity can
be calculated from

$$v_J = \sqrt{2RT_t\frac{\gamma}{\gamma-1}\left(\frac{P_J}{P_s}^{\frac{\gamma-1}{\gamma}} -1\right)} \qquad (7)$$

where P_J is the total pressure measured by the pitot tube
and T_t is the total temperature measured by the thermocouple
inside the model. The initial velocity profile with the
slot height set at 0.015-in. is shown in Figure 9. Several
additional velocity profiles were calculated, with slight
adjustments made to the slot height as necessary to obtain
as uniform a flow as possible. The final velocity profile
is shown in Figure 10.

After pressurizing the model it was mounted on the
sting and pressure tap tubing was attached. All pressure
tap tubing exited from the 1.0625-in. gap between the Coanda
surfaces at the trailing edge of the model. The pressure
tap hoses were carefully routed along the sting to prevent
interference with the force balance. Each hose was checked
for blockage and proper designation.

Several calibration runs were required before testing
began to account for the weight of the model mounted on the
sting. The first of these was the angle-to-volts
calibration described previously. This calibration was done
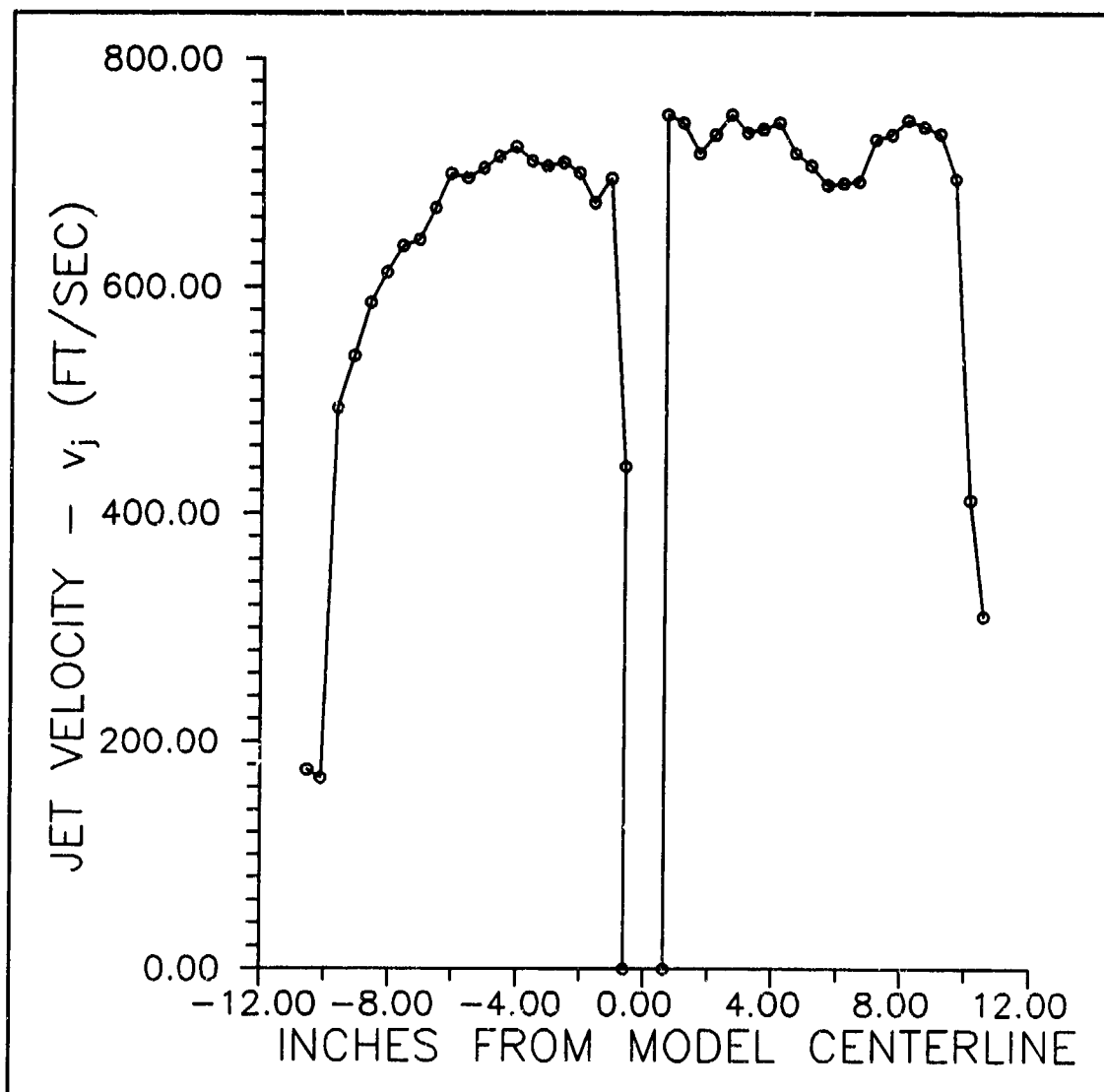with the tunnel off and no blowing air provided. In

22

Figure 9. Velocity Profile Across Slot Before Modifications
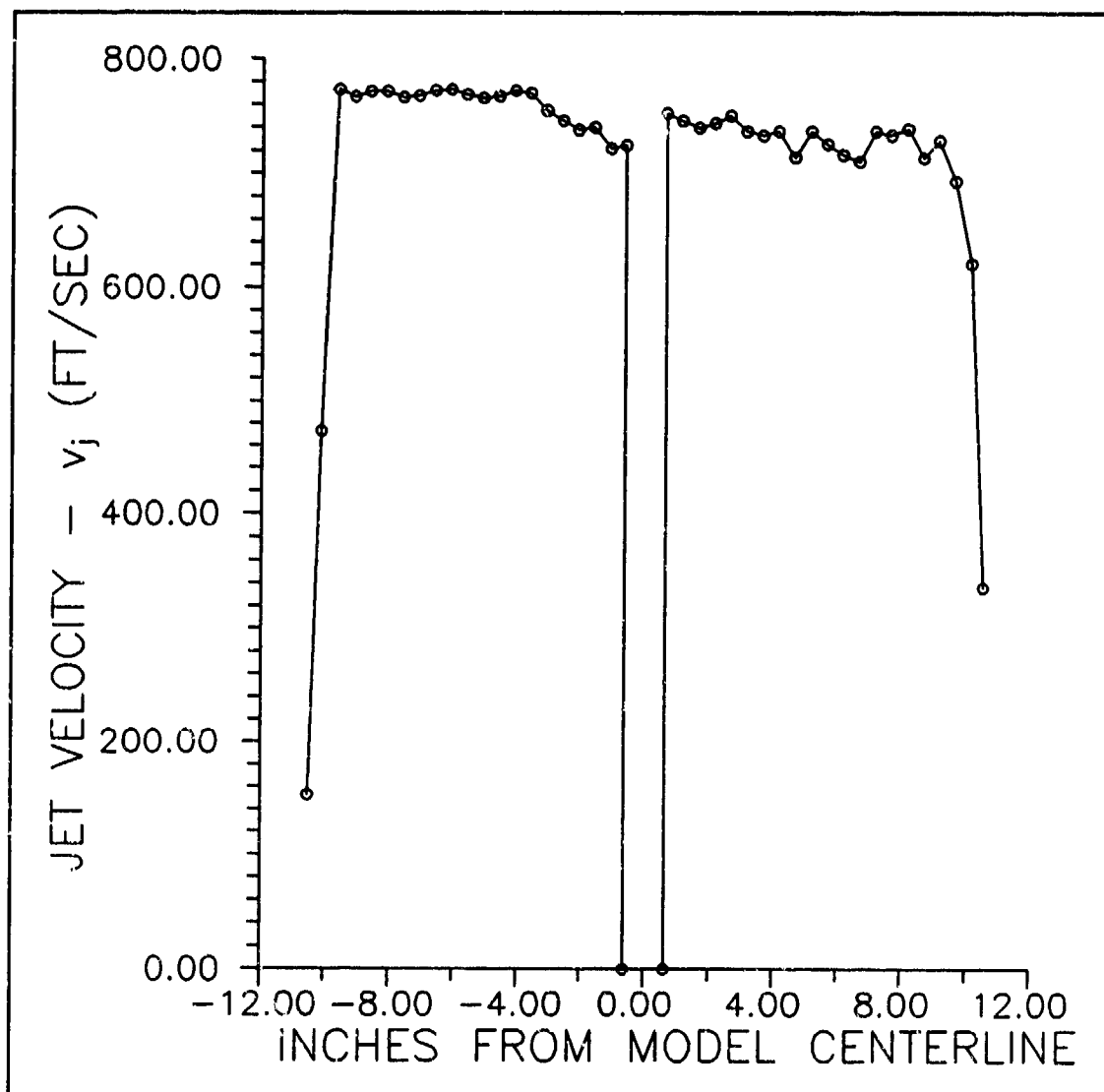with h=0.015-in.

Figure 10.   Velocity Profile Across Slot After Modifications
with ṁ=4.180x10^{-3} slugs/sec

addition to the angle-to-volts curve, tare slopes were required. Force balance data were taken with the wind tunnel off for angles of attack varying from minus six to plus sixteen degrees in two degree increments. This data was used to calculate the model weight and obtain the model center of gravity position referenced to the balance center. These values were stored in a model configuration file and were used during data reduction to account for the weight of the model. Tare slopes were generated for the model both with and without the air supply hose attached.

Preliminary Testing

To account for any contributions to lift and drag on the model caused by the air supply hose, tare runs were made with the hose both on and off. The tunnel was started and a run was made with the air supply hose off and the fiberglass fairing installed on the bottom of the model. Alpha was varied from -6 to +10 degrees in two degree increments. This same run was then made with the air supply hose attached but without any blowing air provided. Values of C_L with the hose unattached and attached are shown as functions of alpha in Figure 11. Similar curves were made for the drag coefficient C_D and the pitching moment C_{Mle}. These are shown in Figure 12 and Figure 13, respectively. The use of these graphs will be explained in the section on data reduction.
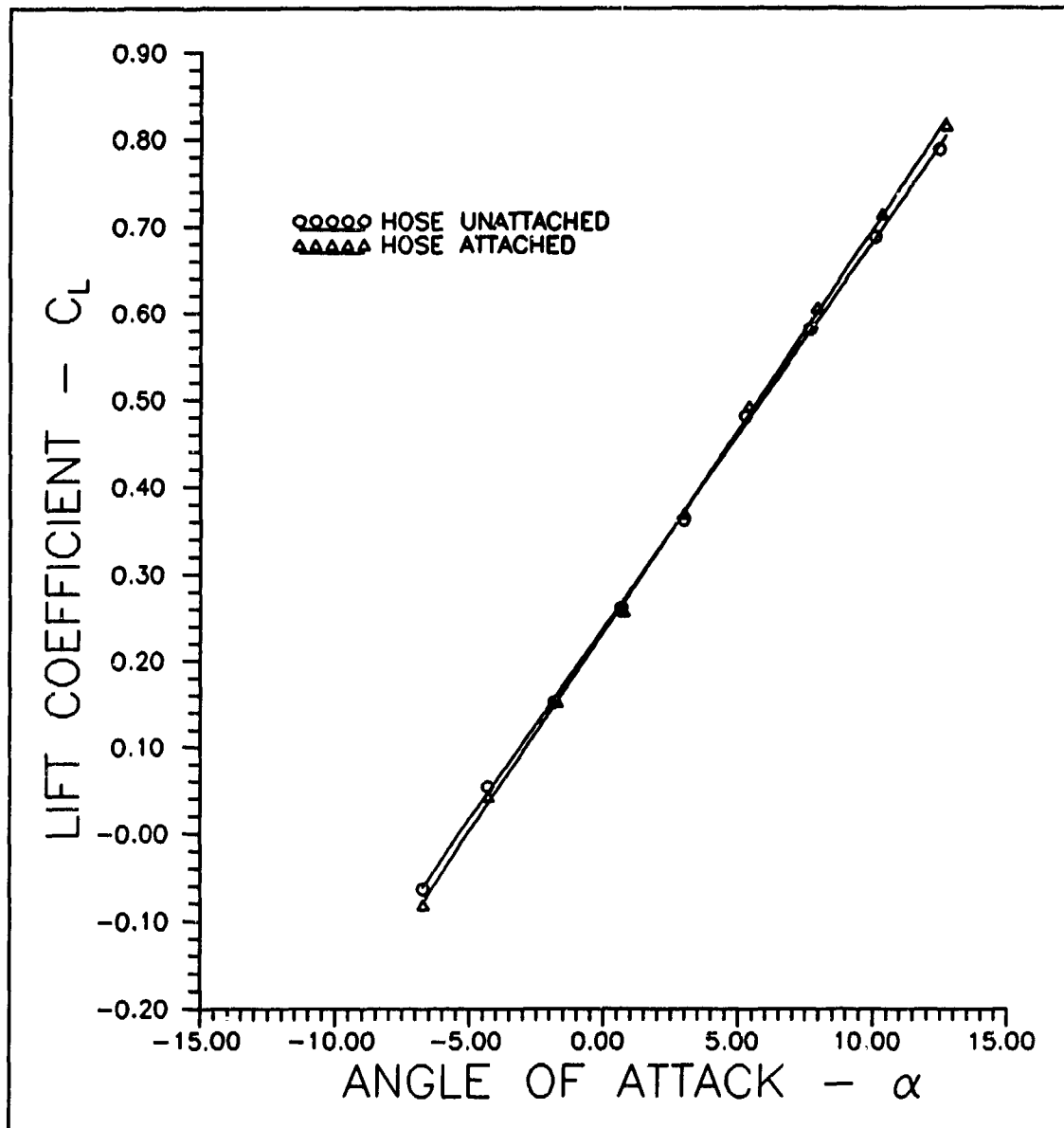
Figure 11.   Lift Coefficient vs. α at RE=9x10^5
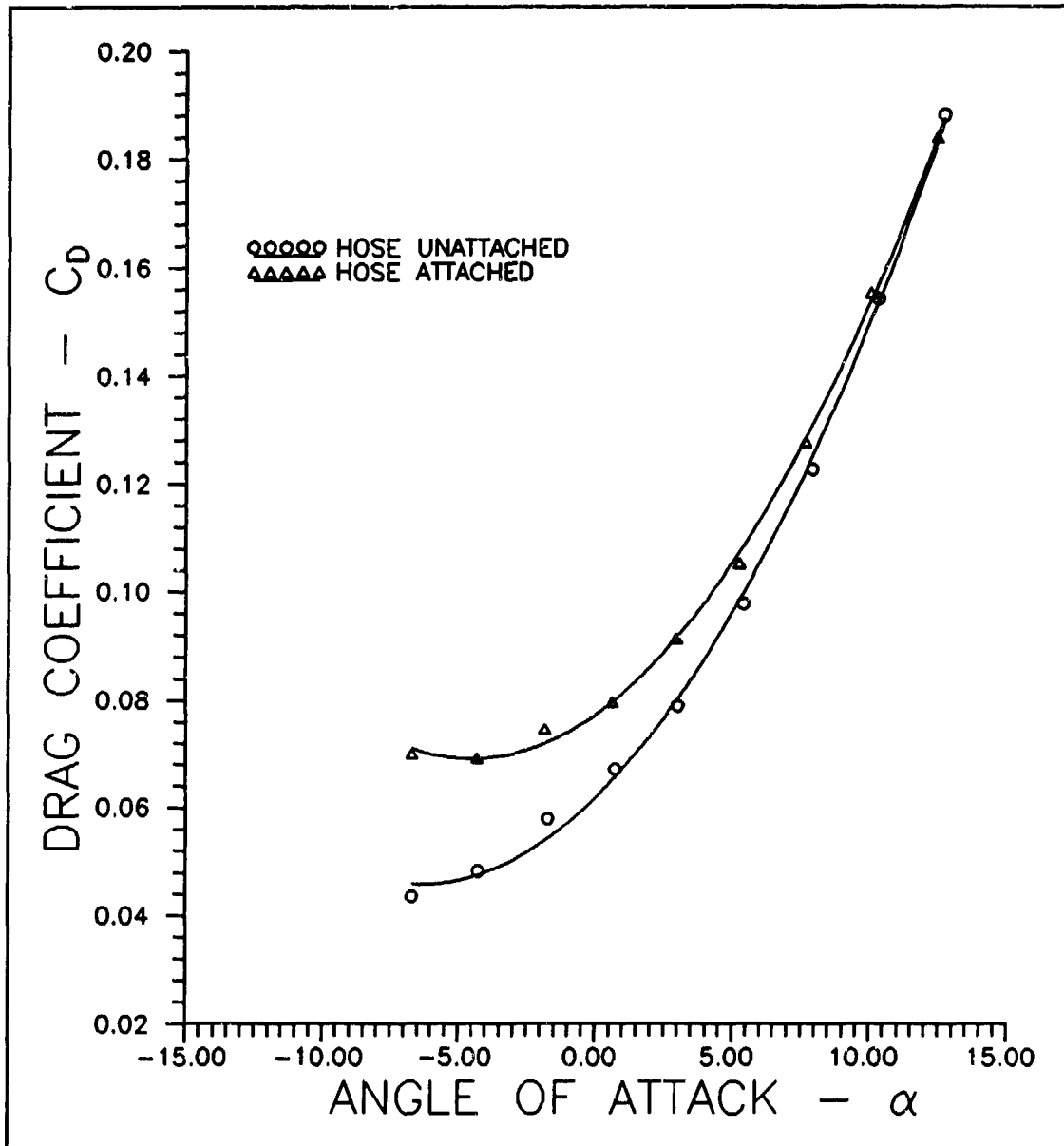
Figure 12. Drag Coefficien vs. α at RE=9x10^5

27
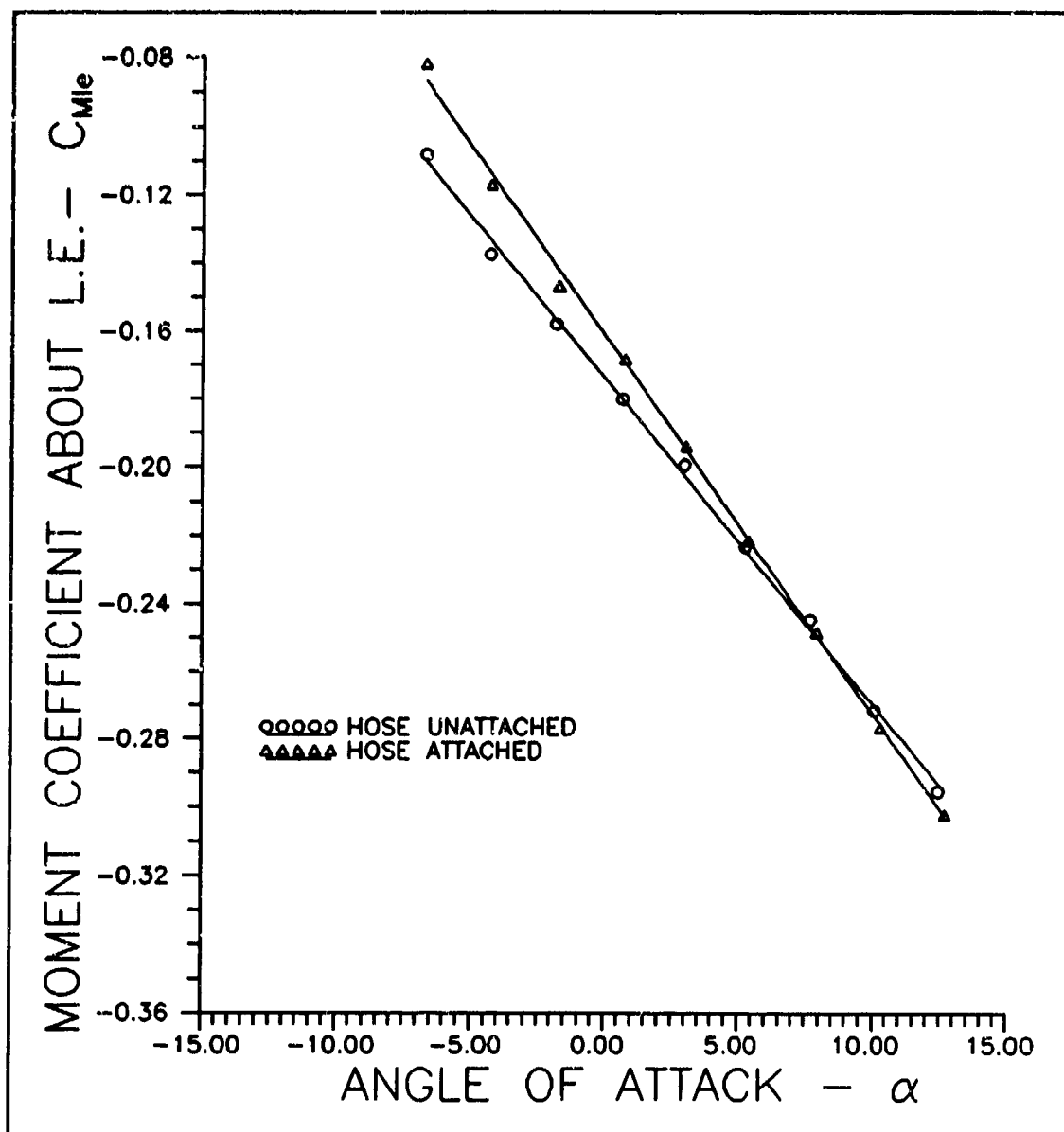
Figure 13.   Moment Coefficient About L.E. vs α at RE=9x10^{5}

A second test required was determining forces on the model with the tunnel off and blowing air provided. For this run the model was set at zero degrees angle of attack and the mass flow rate was varied from zero to maximum. This data was used to correct the aerodynamic coefficients in the final analysis. A plot of normal and axial forces produced as a function of the mass flow rate is shown in Figure 14.

Model Testing

All tests were run at a Reynolds number of $9x10^5$. This equated to a tunnel q between 7.0 and 7.6 inches of H_2O, depending on atmospheric conditions. Runs were made from -6 to +6 degrees alpha in two degree increments. An on-line calibration of the pressure modules was made at the beginning of each run to ensure accuracy of pressure measurements. Testing was accomplished by varying the blowing rate to the model from zero to maximum and back. The mass flow rate was maintained by adjusting the pressure upstream of the venturi with a pressure regulator. At each data point force balance and pressure data were taken using the data acquisition system. The HP-3852A was used to take model plenum chamber and blowing air supply line temperatures. Atmospheric pressure was a manual entry into the Z-248 computer. Pressure tap readings in the mass flow venturi tube and atmospheric temperature were recorded by hand. After the upstream venturi pressure was set,
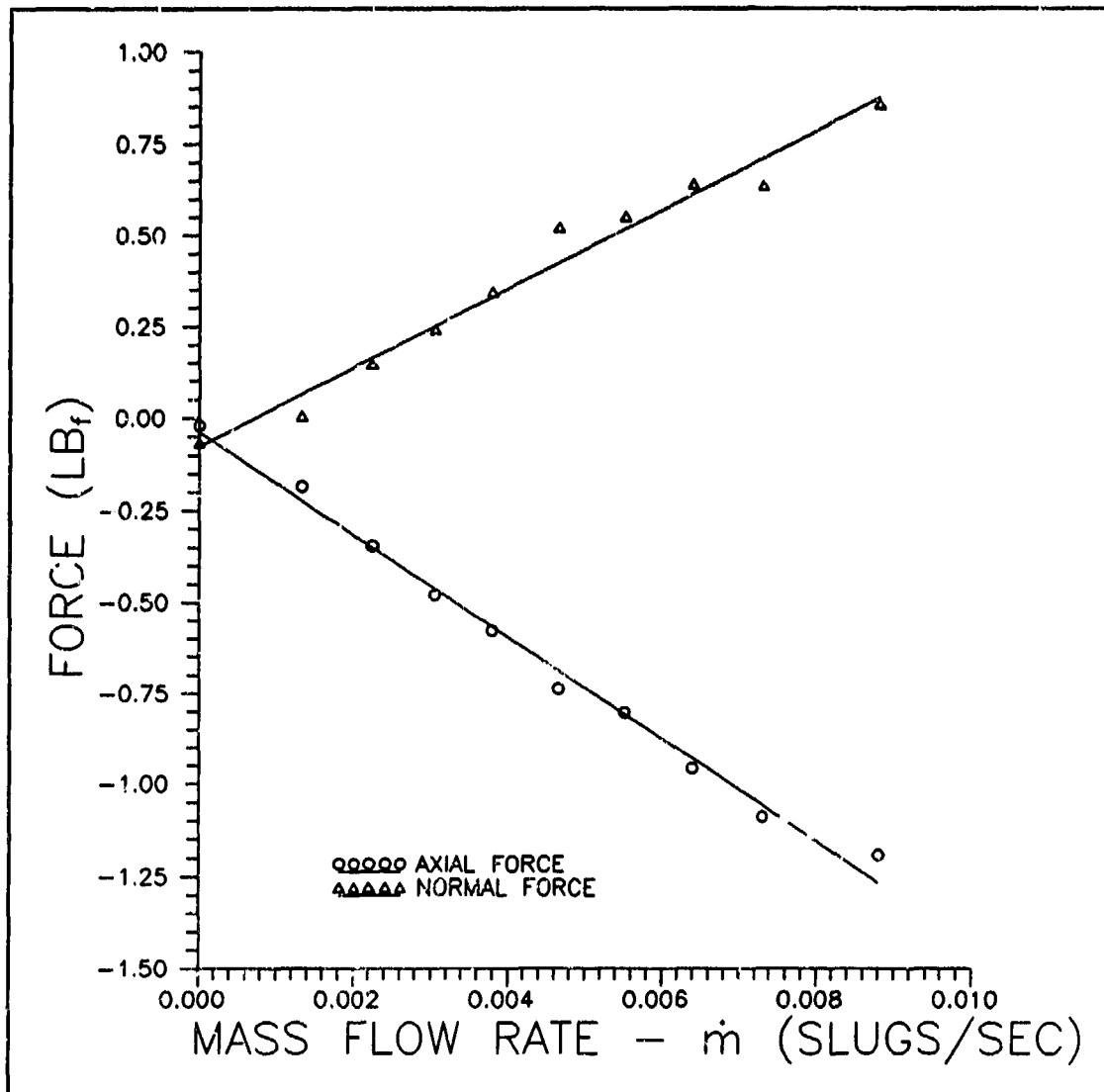
Figure 14.   Forces vs. Mass Flow Rate at RE=0, α=0 Degrees

conditions were allowed to stabilize for one minute to
ensure accuracy of the pressure readings.   After the
completion of the first set of tests the 0, +2, +4, and +6
degree alpha runs were repeated with slightly higher mass
flow rates.

IV. Data Reduction

Data recorded from the acquisition system were reduced to the following coefficients: lift coefficient (C_L), drag coefficient (C_D), moment coefficient about the leading edge (C_{Mle}), pressure coefficient (C_p), and momentum coefficient (C_μ). Aerodynamic forces were referenced to the stability axes. For a description of this axis system see Pope (11:425). Following Englar's work, an equivalent drag coefficient (C_{De}) was computed and used to calculate an equivalent lift-to-drag ratio (4:15).

Momentum Coefficient

The momentum coefficient for a circulation control wing is defined as the momentum of the jet issuing from the slot nondimensionalized by dividing by the dynamic pressure and the wing planform area, thus:

$$C_\mu = \frac{\dot{m} v_j}{q_\infty S} \qquad (8)$$

The jet velocity is calculated by assuming isentropic flow through the slot. Using the relationships

$$\frac{P_t}{P_j} = \left(1 + \frac{\gamma-1}{2} M_j^2\right)^{\frac{\gamma}{\gamma-1}}, \quad \frac{T_t}{T_j} = \left(1 + \frac{\gamma-1}{2} M_j^2\right)$$

$$M_j^2 = \frac{v_j^2}{a_j^2} = \frac{v_j^2}{\gamma R T_j} \qquad (9)$$

31

one can obtain by algebraic manipulation

$$v_j = \sqrt{2RT_t\left[\frac{\gamma}{\gamma-1}\right]\left[1-\left(\frac{P_j}{P_t}\right)^{\frac{\gamma-1}{\gamma}}\right]}$$ (7)

Note that P_j is the static pressure in the jet at the slot exit. To minimize the effects of model geometry v_j is generally calculated assuming expansion to free stream static pressure (14:66). Since the majority of literature calculates v_j in this manner this convention was followed in this report.

The mass flow rate $\dot{m}_j$ was calculated using the static pressures measured upstream of and at the venturi tube throat in the air supply line. The temperature was also required; this was measured using a chromel-alumel thermocouple. Assuming isentropic flow, one obtains (15:194)

$$\dot{m} = \frac{YA_2P_1}{RT_1\sqrt{1-\left(\frac{A_2}{A_1}\right)^2}}\sqrt{2\left(\frac{P_1-P_2}{\gamma}\right)}$$ (11)

The value of Y, known as the expansion factor, is a function of the pressure and area ratios P_2/P_1 and A_2/A_1, respectively. The equation for Y can be found in Reference 15. The area ratio A_2/A_1 is a property of the venturi tube

flow meter; for the venturi tube flow meter used in this
test $A_2/A_1=0.35117$.

Lift Coefficient

The orientation of the two normal force gages N1 and
N2, as well as the axial force gage AX, is shown in
Figure 15. The lift coefficient is defined as

$$C_L = \frac{(N1+N2)\cos\alpha - AX\sin\alpha}{q_\infty S} \qquad (12)$$

The data acquisition software automatically applies weight
tares to the measured values of N1, N2, and AX to account
for the weight of the model. Several corrections were then
made to the computed C_L. A sampling of these corrections
(as well as corrections for C_D and C_{Mle} described later) is
shown in Table 2 for $\alpha=0$. The added lift obtained due to
the jet reaction was found using the force vs. mass flow
rate curve shown in Figure 14. This added force was
nondimensionalized by q_∞ and S.

The graph in Figure 11 was used to correct C_L for the
effects of sting bend and the presence of the air hose.
This data was generated by making an alpha sweep with the
tunnel running and taking force measurements with the air
supply hose unattached. The run was then repeated with the
air supply hose attached but no blowing air supplied.

The value of alpha calculated by the data acquisition
software was greater than the desired angle of attack read
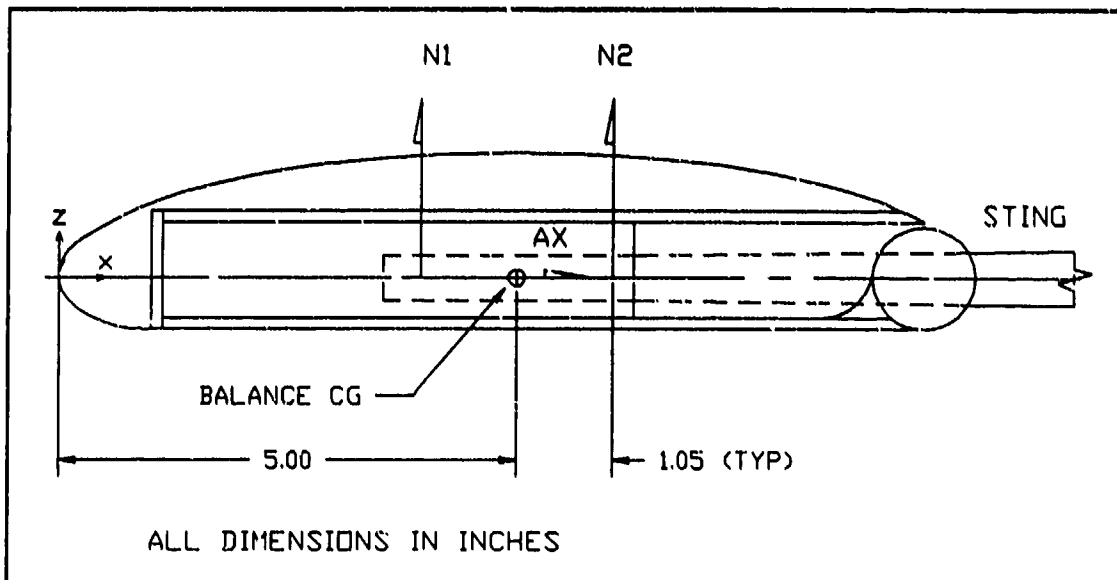
Figure 15. Orientation of Force Gages

off the position potentiometer due to sting bend and had to be corrected. Multiplying the slope of the "HOSE ATTACHED" curve by the change in angle of attack from the desired value provided a second ΔC_L term. A third ΔC_L term was found by calculating the difference between the "HOSE ATTACHED" and the "HOSE UNATTACHED" curves at the desired angle of attack (i.e. -6, -4, +6 degrees). The three ΔC_L corrections were subtracted from the computed C_L to yield a corrected C_L. This corrected C_L represents the lift due to circulation control at a given angle of attack.

Drag Coefficient

Again referring to Figure 15, the drag coefficient is defined as

$$C_D = \frac{(N1+N2)\sin\alpha + AX\cos\alpha}{q_\infty S} \qquad (13)$$

Corrections similar to those made for C_L were made to C_D. The curve shown in Figure 12 was used to correct C_D for the effect of the air hose. No corrections were made to C_D for the effect of the jet reaction.

Equivalent Drag Coefficient

Following Englar's work (4) an equivalent drag term was calculated to take into account the kinetic energy required to produce blowing. This equivalent drag term allows direct comparisons to be made with unblown wings. Since the drag coefficient can be negative at times due to jet reaction forces (although C_D never became negative in this test), the equivalent drag term also serves to avoid unrealistic infinite lift-to-drag ratios for zero drag. Starting with the relationship

$$
\begin{aligned}
D_e &= D_{meas} + \frac{\Delta KE}{v_\infty \Delta time} + \dot{m}v_\infty \\
&= D_{meas} + \frac{\dot{m}v_j^2}{2v_\infty} + \dot{m}v_\infty
\end{aligned}
\qquad (14)
$$

This can be nondimensionalized to

$$C_{D\bullet} = C_D + C_\mu \frac{V_j}{2V_\infty} + C_\mu \frac{V_\infty}{V_j} \tag{15}$$

The second term in the expression accounts for the power required to supply the blowing air, while the last term represents a ram drag inlet penalty.

Pitching Moment About the Leading Edge

Using Figure 15 once more, one can write the equation for the pitching moment about the leading edge. This is

$$C_{Mle} = \frac{-N1(5.0-1.05)-N2(5.0+1.05)}{q_\infty S} \tag{16}$$

The AX force did not contribute to the pitching moment due to the force balance center of gravity being located along the model chord line. Corrections for air supply hose effects and sting bend were applied to C_{Mle} using the graph in Figure 13.

Pressure Coefficient

As mentioned, pressure data were taken for all runs. The pressure coefficient is defined as

$$C_p = \frac{P-P_\infty}{q_\infty} \tag{17}$$

Since the ESP modules read a differential pressure referenced to atmospheric, and tunnel total pressure was

36

assumed equal to atmospheric pressure, one can use the incompressible Bernoulli equation to reduce the above to

$$C_p = \frac{P - P_{atm}}{q_\infty} + 1 \tag{18}$$

Table 2. Representative Data Corrections

$$\alpha = 0, \quad RE = 9 \times 10^5$$

Corrections to C_L

C_μ	measured C_L	air hose	sting bend	jet thrust	C_L
0.000	0.280	-0.003	-0.034	+0.001	0.249
0.003	0.342	-0.003	-0.039	-0.001	0.305
0.008	0.412	-0.003	-0.041	-0.002	0.371
0.013	0.465	-0.003	-0.045	-0.003	0.420
0.019	0.532	-0.002	-0.052	-0.004	0.479
0.025	0.588	-0.002	-0.058	-0.005	0.528
0.033	0.637	-0.002	-0.062	-0.005	0.571
0.040	0.683	-0.002	-0.066	-0.006	0.612
0.049	0.735	-0.001	-0.072	-0.007	0.657
0.058	0.772	-0.001	-0.075	-0.008	0.691
0.069	0.826	-0.001	-0.079	-0.009	0.738
0.079	0.855	-0.001	-0.083	-0.010	0.762
0.092	0.913	-0.001	-0.088	-0.015	0.814
0.103	0.920	-0.001	-0.089	-0.013	0.819
0.117	0.969	-0.001	-0.094	-0.014	0.862

Table 2. continued

Corrections to C_D

C_μ	measured C_D	air hose	sting bend	jet thrust	C_D
0.000	0.068	-0.014	-0.005	------	0.050
0.003	0.069	-0.014	-0.005	------	0.049
0.008	0.076	-0.014	-0.006	------	0.056
0.013	0.083	-0.014	-0.006	------	0.063
0.019	0.093	-0.014	-0.007	------	0.072
0.025	0.106	-0.014	-0.008	------	0.084
0.033	0.120	-0.014	-0.008	------	0.097
0.040	0.129	-0.014	-0.009	------	0.106
0.049	0.144	-0.014	-0.010	------	0.121
0.058	0.155	-0.014	-0.010	------	0.131
0.069	0.173	-0.014	-0.011	------	0.149
0.079	0.186	-0.014	-0.011	------	0.161
0.092	0.201	-0.014	-0.012	------	0.175
0.103	0.209	-0.014	-0.012	------	0.183
0.117	0.226	-0.014	-0.013	------	0.199

Table 2. continued

Corrections to C_{Mle}

C_μ	measured C_{Mle}	air hose	sting bend	jet thrust	C_{Mle}
0.000	-0.174	-0.012	+0.007	------	-0.178
0.003	-0.212	-0.011	+0.008	------	-0.215
0.008	-0.256	-0.011	+0.009	------	-0.258
0.013	-0.289	-0.011	+0.010	------	-0.290
0.019	-0.330	-0.011	+0.011	------	-0.330
0.025	-0.366	-0.011	+0.012	------	-0.364
0.033	-0.397	-0.011	+0.013	------	-0.394
0.040	-0.426	-0.010	+0.014	------	-0.422
0.049	-0.460	-0.010	+0.015	------	-0.455
0.058	-0.484	-0.010	+0.016	------	-0.478
0.069	-0.517	-0.010	+0.017	------	-0.510
0.079	-0.536	-0.010	+0.018	------	-0.528
0.092	-0.572	-0.010	+0.019	------	-0.563
0.103	-0.578	-0.010	+0.019	------	-0.568
0.117	-0.608	-0.010	+0.020	------	-0.597

Wind Tunnel Corrections

Several corrections for wind tunnel effects were applied to the test data during data reduction. These corrections are explained in Pope (Reference 11), and include solid blockage, buoyancy, wake blockage, and downwash corrections. Solid blockage occurs primarily in closed-section tunnels. The presence of the model causes a curvature of the streamlines around the model, particularly near the edges of the tunnel. This squeezing of the streamlines causes an increase in the effective dynamic pressure in the tunnel, and hence an increase in all forces and moments on the model. Buoyancy effects are due to the tunnel boundary layer thickening as the air moves downstream. This thickening reduces the tunnel cross-sectional area, causing an increase in the velocity of the tunnel at the test section. This increased velocity in turn leads to a reduced pressure in the tunnel as the air moves downstream, which is a favorable pressure gradient. This pressure gradient tends to draw the model downstream, affecting drag measurements. Wake blockage affects primarily drag measurements, and is similar to solid blockage. Since the velocity in the wake is less than freestream velocity, to satisfy continuity the velocity outside the wake must be greater then freestream. This results in a favorable pressure gradient, which again tends to draw the model downstream. The final correction was for

downwash effects. The presence of the tunnel walls in an enclosed test section tends to diminish the downwash from a wing, which leads to a reduction in the induced drag.

Although not considered a tunnel boundary correction, one other correction was made for dynamic pressure "skew" and applied during the reduction process. Previous research in the AFIT tunnel discovered the dynamic pressure calculated from the static ports at the mouth of the tunnel differed from the measured tunnel q in the test section by a factor of 1.019 (12:18). This factor was applied during data reduction.

V. Results and Discussion

Preliminary Testing

Initial testing was concerned with establishing uniform flow across the left and right slots. Initially the slot heights were set to 0.015-in. using a feeler gauge. Using the pitot tube and traversing rod arrangement discussed previously, a velocity profile across the slot was produced. The original profile with the slot height fixed at 0.015-in. is shown in Figure 9. Although velocities were fairly high for the blowing rate (4.125×10^{-3} slugs/sec) the uniformity across each slot was poor, varying from 168-722 ft/sec across the left slot (as seen looking forward) and from 310-750 ft/sec across the right slot. The lowest velocities were encountered at the edge of each slot out near the wing tips. Due to the design of the model the slot height was not adjustable at the edge of the slot, and hence the low velocities were accepted as unavoidable at these positions. Since uniform jet velocity across the slot was considered necessary for this test, the slot height was then adjusted to produce a more uniform profile. This resulted in the velocity profile shown in Figure 10. Although the plenum chambers contained small teardrop shaped mounting blocks for the slot adjusting screws (Figure 4 and Figure 5) there were no noticeable velocity variations behind the blocks.

Tuft studies done on the Coanda surface showed no significant spanwise flow in the jet sheet and strong

43

attachment of the jet sheet through 90 degrees as measured clockwise from the vertical (i.e. attachment up to the trailing edge). Pressure data taken for increasing blowing rates with the tunnel on showed a favorable pressure gradient maintained on the Coanda surface up to 90 degrees from the vertical, with the onset of an adverse pressure gradient past that angle. This data agrees with Harvell, who was using a similar model cross section (Reference 7).

Primary Testing

Lift coefficient vs. momentum coefficient data are shown in Figure 16 for alpha varying from -6 to +6 degrees. This data follows the trend for circulation control wings. The initial slope of the lift curve is due to the jet reenergizing the boundary layer and delaying separation, while the gradual flattening of the curve represents supercirculation. Supercirculation is defined by Englar as a "large stagnation point movement and greater circulation than that obtained solely by entraining the boundary layer" (14:2). There appears to be little dependence on angle of attack of the rate of lift augmentation, defined as dC_L/dC_μ.

Using a correction for 3D airfoils developed by Maskall and Spence and presented in Reference 16, along with McCormick's (17:201) correction for partial span blowing and thickness ratio allowed a comparison of data with 2D data

44

presented by Harvell (7:53). A factor F that corrects for aspect ratio and momentum coefficient is given by

$$F = \frac{AR + 2C_\mu/\pi}{AR + 2 + 0.604 C_\mu^{0.5} + 0.876 C_\mu} \tag{19}$$

where AR is the aspect ratio of 2.235. Additional corrections suggested by McCormick for partial span blowing are

$$\lambda = \frac{S'}{S}$$
$$\nu = \frac{S'(\partial C_l/\partial \alpha) + (S-S')(\partial C_l/\partial \alpha), C_\mu = 0}{S(\partial C_l/\partial \alpha)} \tag{20}$$

where S' is the wing area affected by blowing, and S is the total wing area. These factors, along with a thickness factor of (1 + t/c), where t/c is the model thickness ratio of 0.196, produce the equation to convert section lift coefficients to 3D lift coefficients:

$$C_L = F(1 + t/c)(\lambda C_{l_{(C_\mu, \alpha = 0)}} + \nu C_{l_\alpha} \alpha) + C_{L_{(C_\mu = 0, \alpha = 0)}} \tag{21}$$

The value for C_L at $C_\mu = 0$, $\alpha = 0$ was taken from Figure 16 and was equal to 0.2495. Theoretical and experimental lift coefficients vs. momentum coefficient data are shown in Figure 17. The predicted 3D lift coefficients were approximately twice the measured lift coefficients,
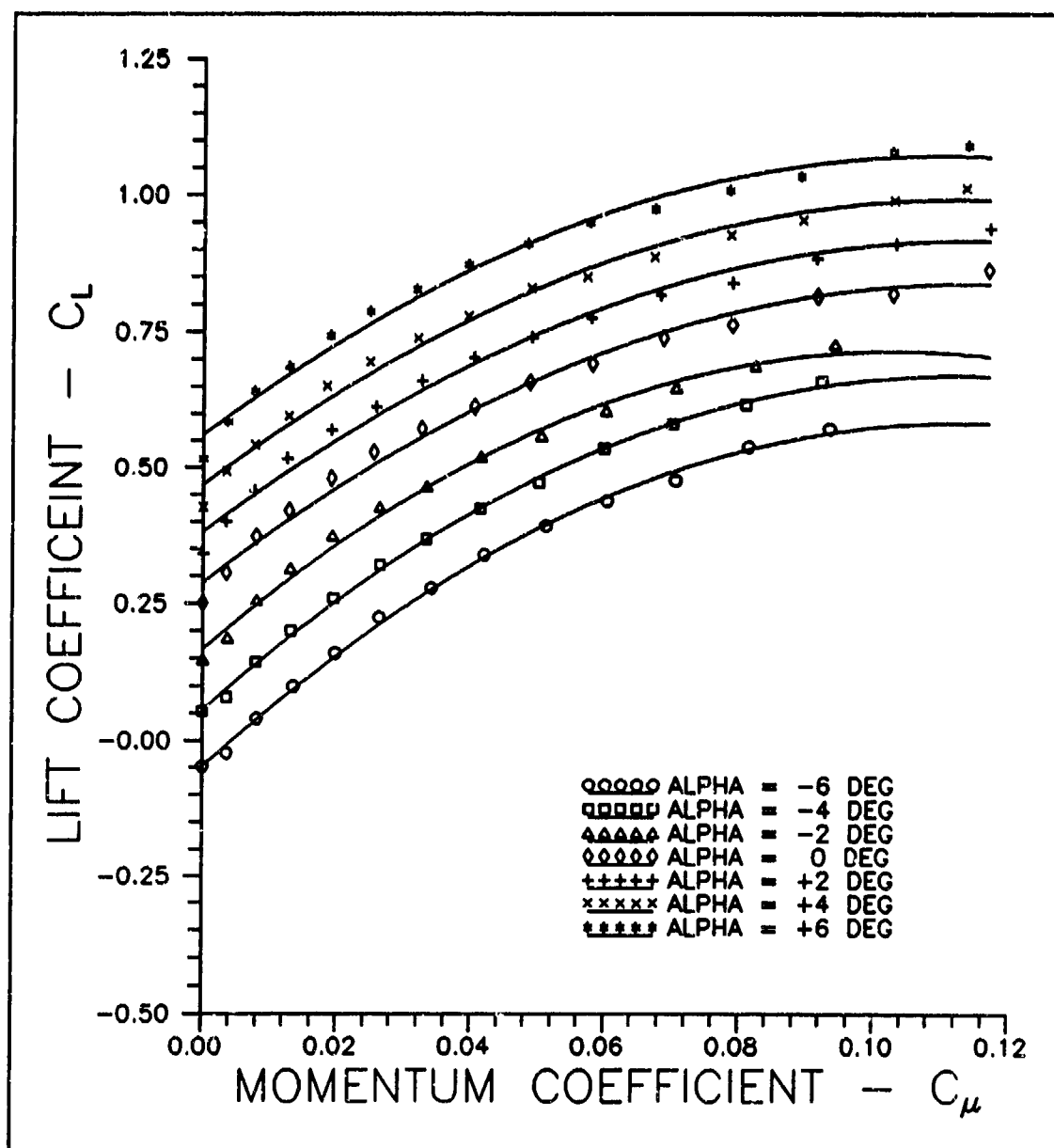
45

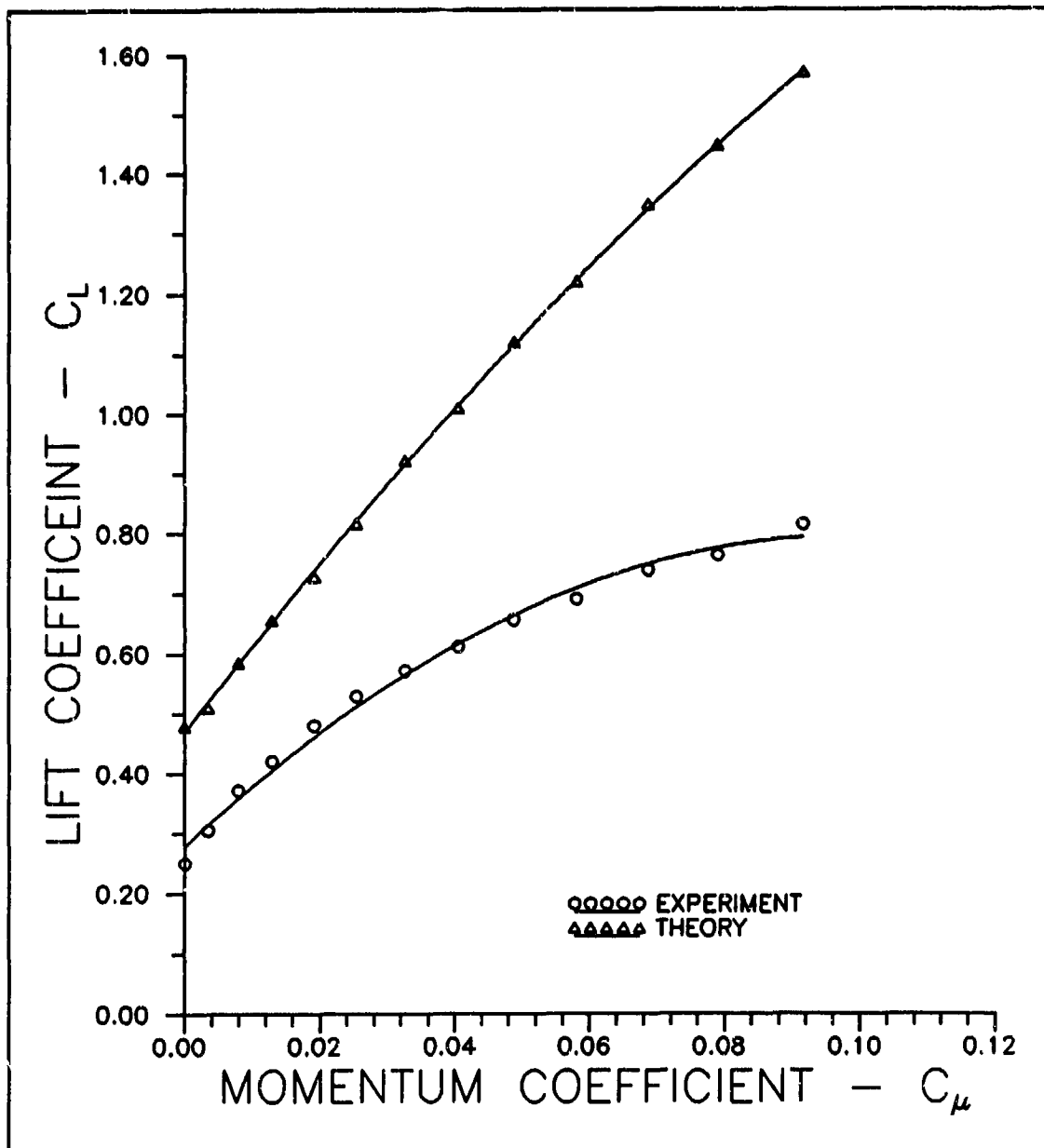Figure 16. Lift Coefficient vs. Momentum Coefficient at RE=9x10^5

Figure 17. Theoretical and Experimental C_L vs. Momentum Coefficient at $\alpha = 0$

particularly at higher blowing rates. The reason for this is unclear. Previous comparisons of 2D airfoils and 3D wings using these corrections have shown good agreement (16:14).

Pressure data for C_μ=0, 0.040, and 0.117 and α=0 degrees are shown in Figure 18, Figure 19, and Figure 20, respectively. This data was taken from a row of pressure taps located 6-in. from the left wing tip. Additional taps located at 10-in. from the left wing tip and 6-in. from the right wing tip verified the spanwise uniformity of the flow. At zero blowing rate a strong suction peak formed at the leading edge on the bottom surface as the flow accelerated around the blunt leading edge. This suction peak was decreased as the blowing rate increased, possibly due to the forward stagnation point moving toward the bottom surface of the wing as supercirculation was achieved. The leading edge suction peak was gradually replaced by an increasing suction peak at the trailing edge. This trailing edge suction peak gradually moved around the Coanda surface as C_μ was increased until it was located right at the trailing edge, signifying attached flow was maintained at least 90 degrees from the vertical. Once past 90 degrees, however, a strong adverse pressure led to separated flow.
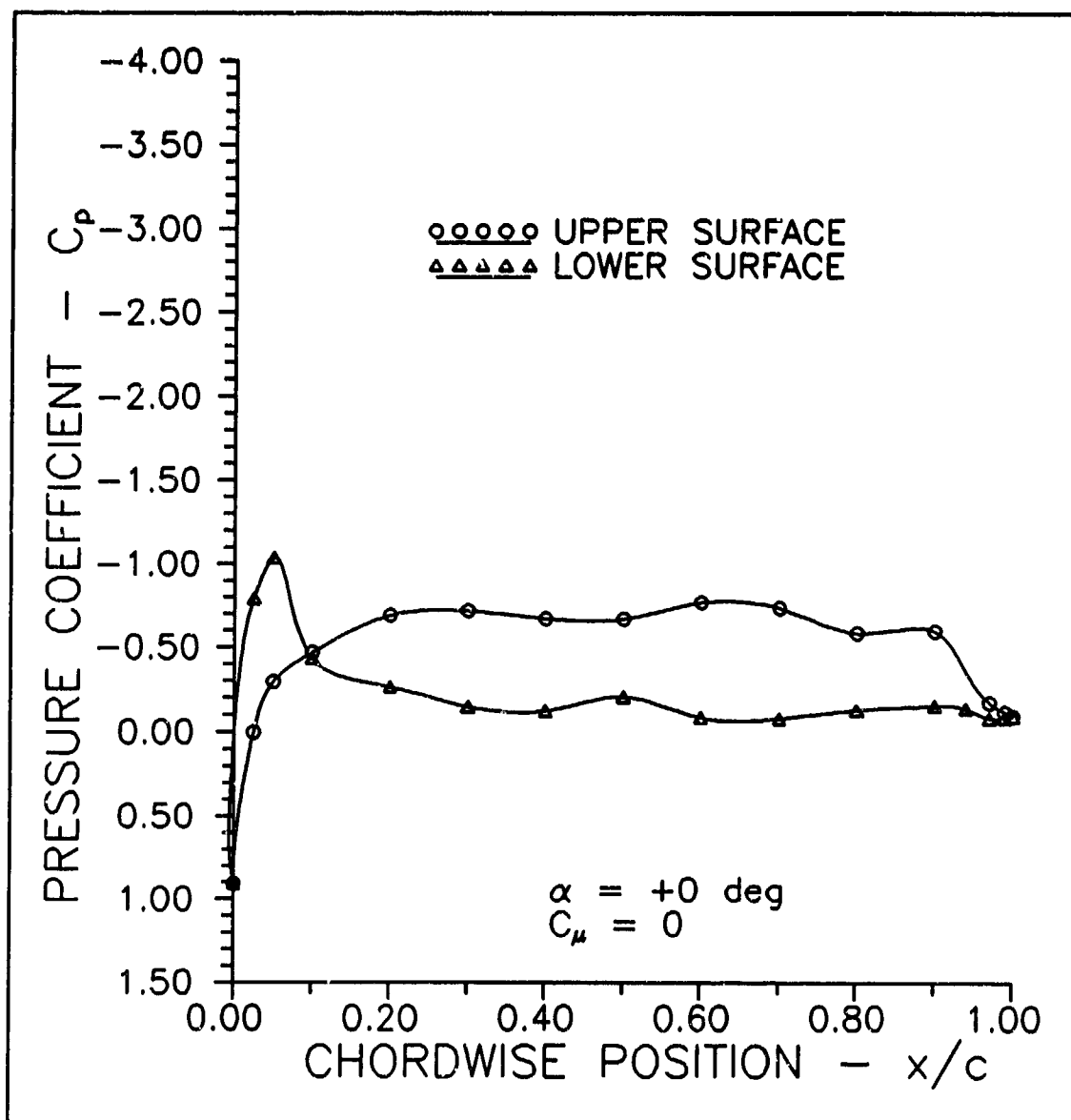
Figure 18.   Pressure Coefficient vs. Chordwise Position
for RE=9×10^5, C_μ=0.000, α=0 Degrees
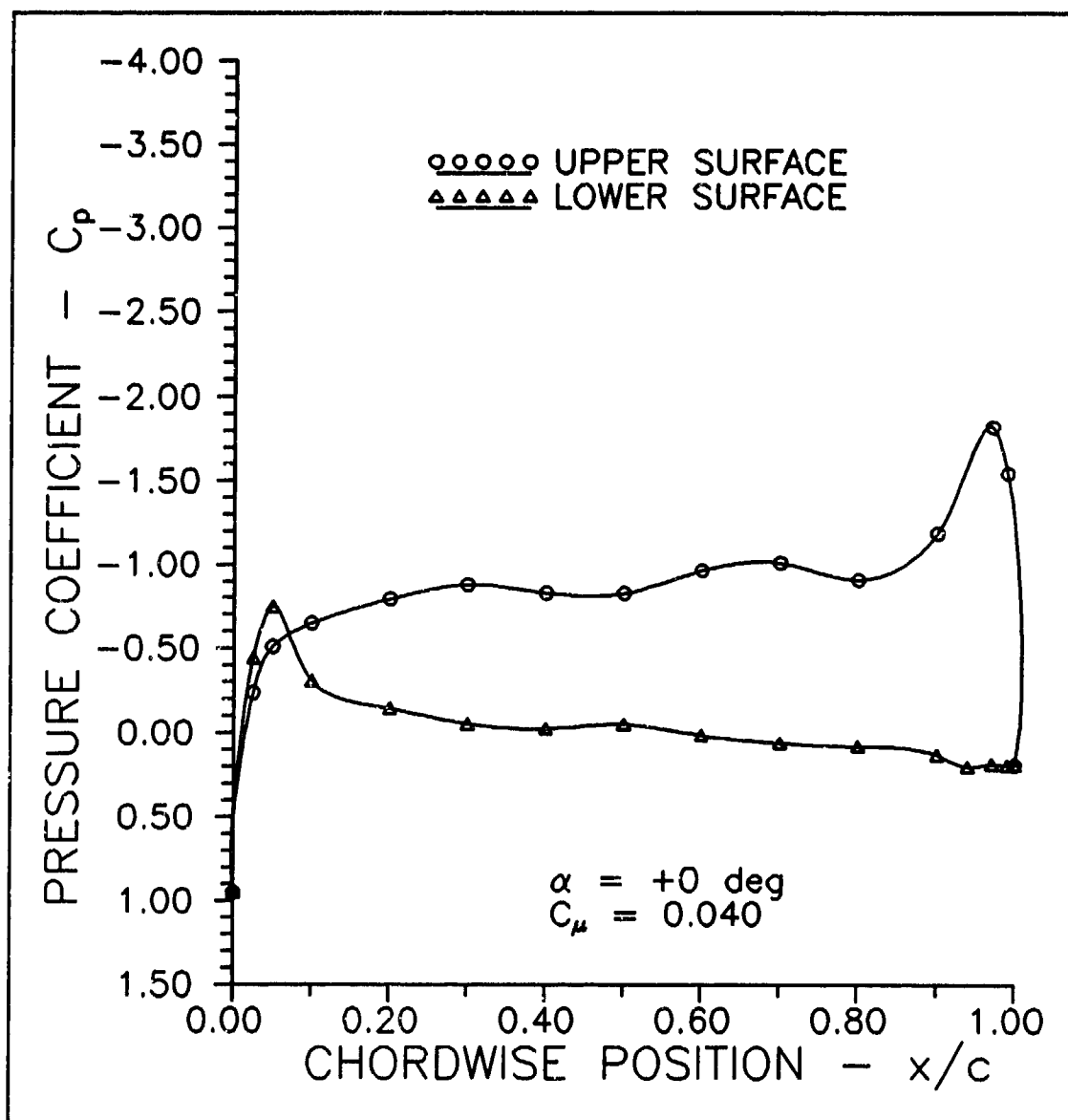
49

Figure 19. Pressure Coefficient vs. Chordwise Position
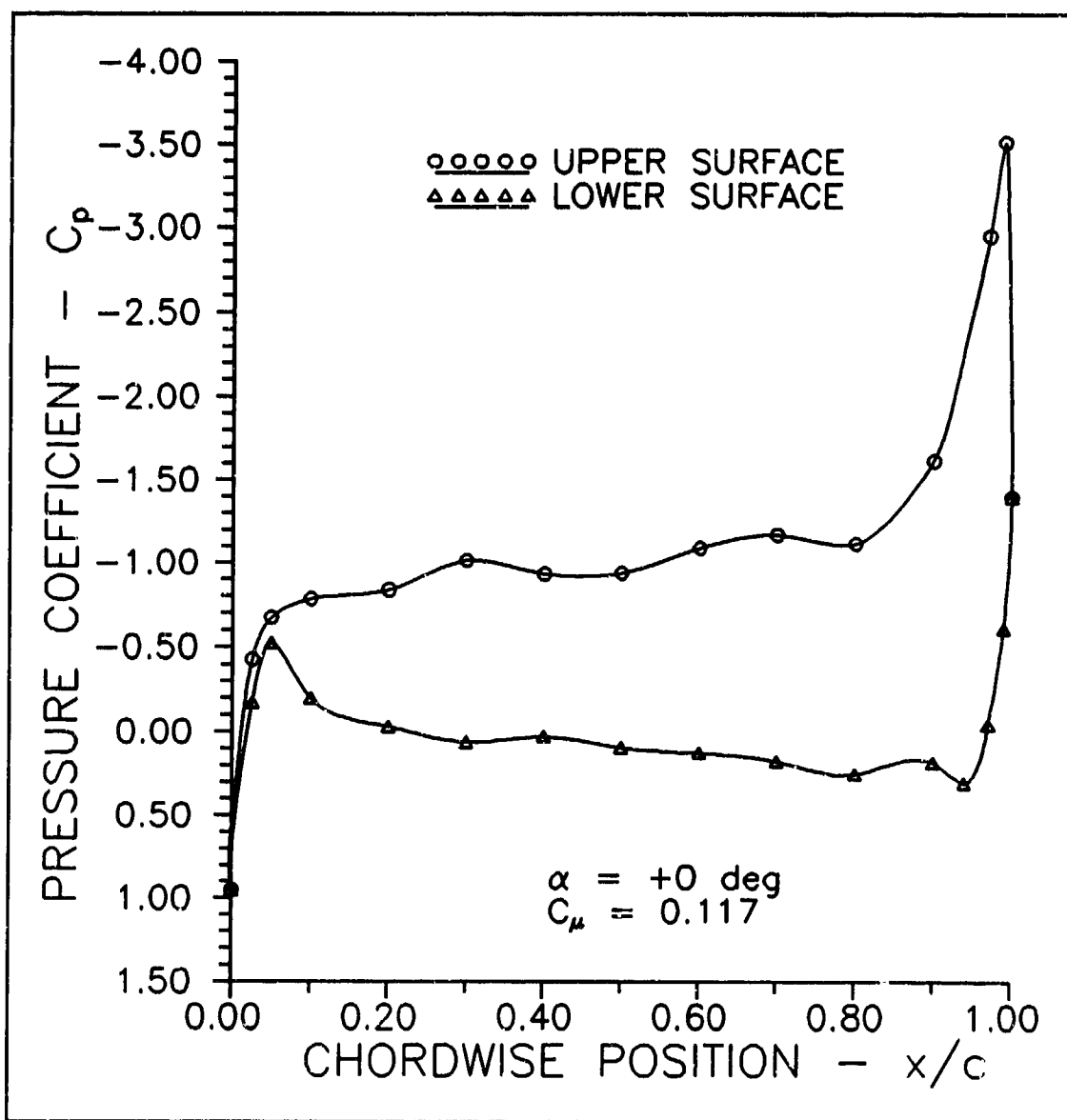for RE=9×10^5, C_μ=0.040, α=0 Degrees

50

Figure 20.   Pressure Coefficient vs. Chordwise Position
             for RE=9x10^5, C$_\mu$=0.117, α=0 Degrees

51

Corrected drag coefficient vs. momentum coefficient data are shown in Figure 20. This data is very atypical of circulation control wings, and could be caused by the air supply hose (which was taped to the sting) restricting axial force measurements made by the force balance. Circulation control wings tend to have high drag coefficients at low blowing rates. This is due to their blunt trailing edge causing separated flow and a resulting momentum deficit behind the wing. At higher blowing rates the drag tends to decrease, due to separation being delayed through boundary layer control. The drag can be negative at times, due to the force from the jet reaction being greater than drag forces produced by the blunted trailing edge. The strong Coanda turning of the model appears to be reducing the jet reaction--turning the resultant force vector down, increasing the normal force but adding very little axial force. This is borne out by the low jet reaction axial forces generated in the force vs. mass flow rate graph shown in Figure 14.

Pitching moment data about the leading edge are shown in Figure 22. The large nose down pitching moments are due to the strong suction peak at the trailing edge and are characteristic of circulation control wings. The change in pitching moment coefficient with a change in momentum coefficient appeared to be independent of the angle of attack.

Lift-to-equivalent drag coefficient vs. lift coefficient data are presented in Figure 23 for various angles of attack. These curves are typical of circulation control wings. The lift-to-equivalent drag ratio peak in each graph occurs primarily as a result of the definition of the equivalent drag discussed earlier. Since the C_μ term contains a v_j term, it can be seen that the second term in the equivalent drag equation increases as $(v_j/v_\infty)^3$, and quickly dominates. The effect of this is that maximum efficiency for circulation control wings occurs at lower blowing rates, and not at the point of maximum C_L.

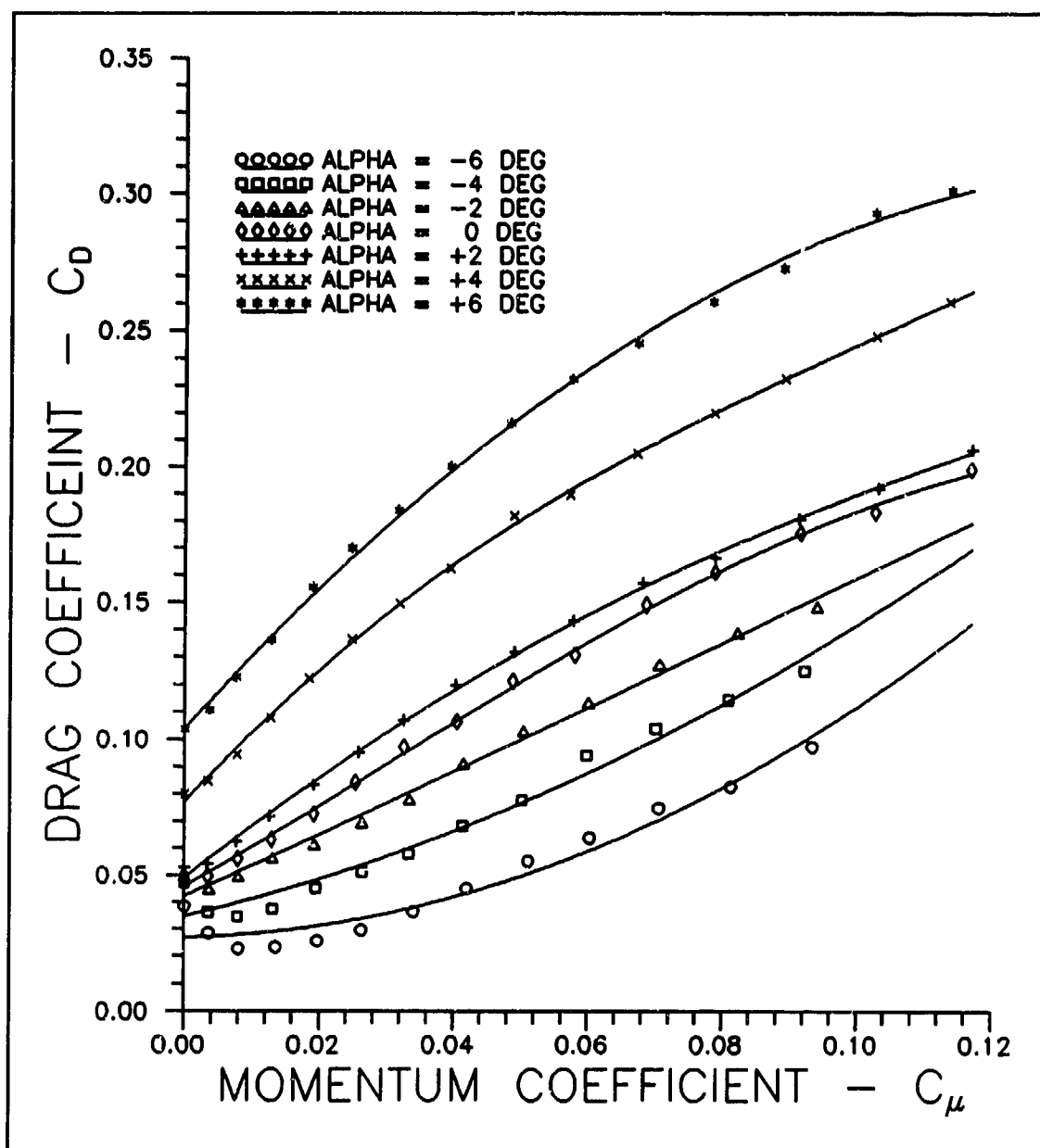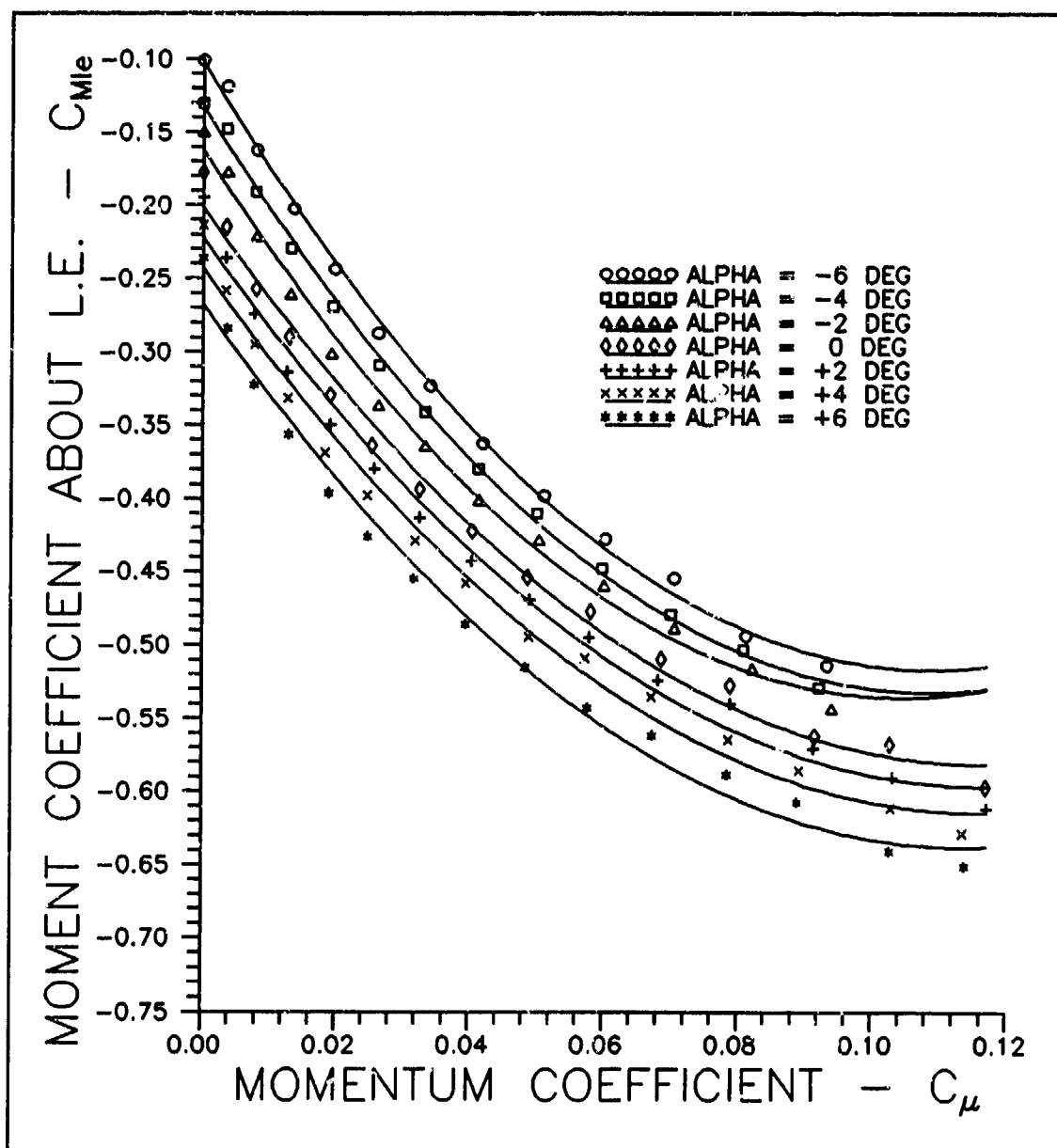Figure 21.   Drag Coefficient vs. Momentum Coefficient
              at RE=9x10^5

54

Figure 22. Moment Coefficient About L.E. vs. Momentum
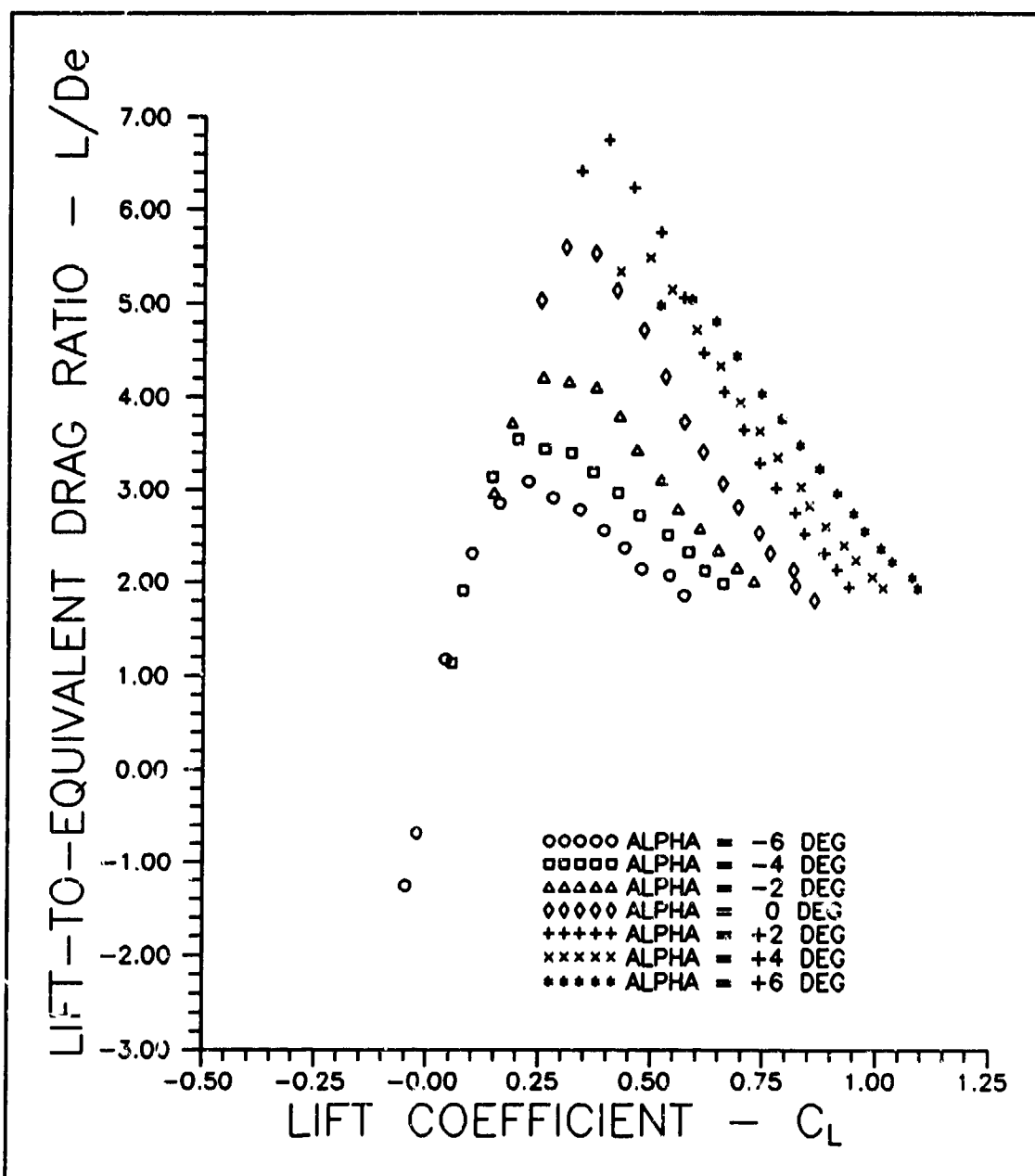Coefficient at RE=9x10^5

Figure 23. Lift-to-Equivalent Drag Ratio vs. Lift Coefficient at $RE=9 \times 10^5$

VI. Conclusions

1. Testing of circulation control wings appears to be feasible using a sting if proper corrections are made to the collected data and care is taken to avoid interference with the force balance from the air supply hose. Trends were generally in accordance with 2D data, with the exception of the drag coefficient, which gave results opposite of what is the norm for circulation control wings.

2. Lift coefficients were somewhat lower than 2D data and theory suggested they should be. This was perhaps a result of the low aspect ratio of the model and unknown downwash effects. It's also possible the lift coefficients were lower than expected due to interference from the air supply hose.

3. Good Coanda surface turning and adequate momentum coefficients were achieved with the available air supply. Fairly uniform slot velocities were achieved despite having two separate plenum chambers in the model.

VII. Recommendations

1. Further testing on the model should be accomplished. An investigation of slot height effect on performance is warranted.

2. Testing should also include Reynolds number effects. Lower Reynolds numbers would allow higher momentum coefficients due to lower free stream dynamic pressure.

3. A new method of supplying blowing air to the model should be investigated, perhaps through a blowing sting. The presence of the air hose attached to the model and the sting may have affected force readings.

4. A means of performing check loads on the force balance with the model installed and the air supply hose attached should be developed. Although check loads were made on the force balance without the model installed, only limited check loads could be accomplished with the model installed on the sting. This was due to the lack of a calibration harness that could load the model throughout the range of expected forces without damaging it. A means of loading the force balance throughout the expected force range with a model installed and all air supply hoses connected should be investigated.

Bibliography

1. Kind, R.J. and D.J. Maull. "An Experimental Investigation of a Low-Speed Circulation-Controlled Aerofoil," _The Aeronautical Quarterly_, 19: 170-182 (May 1968).

2. Williams, R.M. and H.J. Howe. _Two-Dimensional Subsonic Wind Tunnel Tests on a 20-Percent Thick, 5-Percent Cambered Circulation Control Airfoil_. NSRDC Technical Note AL-176. Bethesda, MD: Naval Ship Research and Development Center, August 1970.

3. Englar, R.J. _Two-Dimensional Subsonic Wind Tunnel Tests of Two 15-Percent Thick Circulation Control Airfoils_. NSRDC Technical Note AL-211. Bethesda, MD: Naval Ship Research and Development Center, August 1971.

4. Englar, R.J. _Two-Dimensional Subsonic Wind Tunnel Investigations of a Cambered 30-Percent Thick Circulation Control Airfoil_. NSRDC Technical Note AL-201. Bethesda, MD: Naval Ship Research and Development Center, May 1972.

5. Loth, J.L. et al. "Flight Performance of a Circulation Controlled STOL Aircraft," _Journal of Aircraft_, 13:169-173 (March 1976)

6. Grumman Aerospace Corporation. _Design of an A-6A Flight Demonstrator Aircraft Modified with a Circulation Control Wing (CCW)_. NSRDC Report CCW/1255-RE-01. Bethesda, MD: Naval Ship Research and Development Center, January 1978.

7. Harvell, Captain John K. _An Experimental/Analytical Investigation into the Performance of a 20-Percent Thick, 8.5 Percent Cambered Circulation Controlled Airfoil_. MS Thesis, AFIT/GAE/AA/82D-13. School of Engineering, Air Force Institute of Technology (AU), Wright-Patterson AFB OH, December 1982 (AD-124732).

8. Franke, M.E. and J.K. Harvell. "Wind Tunnel Studies of Circulation Control Elliptical Airfoils," School of Engineering, Air Force Institute of Technology (AU), Wright-Patterson AFB OH.

9. Trainor, Captain John W. _A Wind Tunnel Study of a Sting-Mounted Circulation Control Wing_. MS Thesis, AFIT/GAE/ENY/89D-38. School of Engineering, Air Force Institute of Technology (AU), Wright-Patterson AFB OH, December 1989.

10. Wood, N. and J. Nielsen. <u>Circulation Control Airfoils Past, Present, and Future</u>. AIAA Paper 85-0204. American Institute of Aeronautics and Astronautics, January 1985.

11. Pope, A. and W.H. Rae. <u>Low Speed Wind Tunnel Testing</u>. New York: John Wiley & Sons, Inc., 1984.

12. Systems Research Laboratories. <u>AFIT 5-ft Wind Tunnel Data Acquisition System</u>. Version 1.3, User's Manual. Wright-Patterson AFB OH, April 1990.

13. Pressure Systems, Inc. <u>Model 780B/T Pressure Measurement System User's Manual</u>. First Edition, September 1983.

14. Englar, R.J. <u>Experimental Investigation of the High Velocity Coanda Wall Jet Applied to Bluff Trailing Edge Circulation Control Airfoils</u>. NSRDC Technical Report 4708. Bethesda, MD: Naval Ship Research and Development Center, September 1975.

15. Vennard, J.K. and R.L. Street. <u>Elementary Fluid Mechanics</u>. New York: John Wiley & Sons, Inc., 1982.

16. Henderson, C. <u>An Engineering Method for Estimating the Aerodynamic Characteristics of Circulation Control Wings (CCW)</u>. NADC Report 82186-60. Warminster, PA: Naval Air Development Center, June 1982.

17. McCormick, B.W. Jr. <u>Aerodynamics of V/STOL Flight</u>. Orlando: Academic Press, 1967.

Vita

Captain Michael E. Pelletier was born on 6 February 1960 in Livonia, Michigan. He graduated from Stevenson High School in Livonia in 1978. In 1984 he graduated from the University of Michigan with a Bachelor of Science degree in Aerospace Engineering and was commissioned through the Reserve Officer Training Corps program. From May of 1985 to March of 1986 he attended Euro-NATO Joint Jet Pilot Training until he was medically disqualified. After graduating from the Aircraft Maintenance Officer's Course at Chanute Air Force Base, Illinois in September 1986, he served as an F-16/RF-4C aircraft maintenance officer with the 363d Tactical Fighter Wing at Shaw Air Force Base, South Carolina. Before coming to the Air Force Institute of Technology he was the officer-in-charge of the Maintenance Branch, 363d Equipment Maintenance Squadron, 363d Tactical Fighter Wing. In May of 1989 Captain Pelletier transferred to the School of Engineering, Air Force Institute of Technology, Wright-Patterson AFB, Ohio.

Permanent address: 9872 22 Mile Rd.
                     Sand Lake, MI 49343

REPORT DOCUMENTATION PAGE

Public reporting burden for this collection of information is estimated to average 1 hour per response, including the time for reviewing instructions, searching existing data sources, gathering and maintaining the data needed, and completing and reviewing the collection of information. Send comments regarding this burden estimate or any other aspect of this collection of information, including suggestions for reducing this burden, to Washington Headquarters Services, Directorate for Information Operations and Reports, 1215 Jefferson Davis Highway, Suite 1204, Arlington, VA 22202-4302, and to the Office of Management and Budget, Paperwork Reduction Project (0704-0188), Washington, DC 20503.

1. AGENCY USE ONLY (Leave blank)	2. REPORT DATE December 1990	3. REPORT TYPE AND DATES COVERED Master's Thesis

4. TITLE AND SUBTITLE
AN EXPERIMENTAL STUDY OF A STING-MOUNTED SINGLE-SLOT CIRCULATION CONTROL WING

5. FUNDING NUMBERS

6. AUTHOR(S)
Michael E. Pelletier, Captain, USAF

7. PERFORMING ORGANIZATION NAME(S) AND ADDRESS(ES)
Air Force Institute of Technology
WPAFB OH 45433-6583

8. PERFORMING ORGANIZATION REPORT NUMBER
AFIT/GAE/ENY/90D-18

9. SPONSORING/MONITORING AGENCY NAME(S) AND ADDRESS(ES)

10. SPONSORING/MONITORING AGENCY REPORT NUMBER

11. SUPPLEMENTARY NOTES

12a. DISTRIBUTION/AVAILABILITY STATEMENT
Approved for public release; distribution unlimited

12b. DISTRIBUTION CODE

13. ABSTRACT (Maximum 200 words)

This wind tunnel study investigated the feasibility of using a sting and force balance to measure the aerodynamic forces and moments on a circulation control wing. A 20% thick, 8.5% camber, single blowing slot, rectangular wing was designed, built, and tested in the AFIT 5-ft wind tunnel. Lift and drag coefficients were referenced to the stability axis. The Reynolds number for all tests was 9×10^5; angle of attack was varied from -6 to +6 degrees. Trends in the data were similar to two dimensional data, with the exception of high drag coefficients with increased blowing. Results show it is feasible to test three dimensional wings using a sting and force balance if appropriate data corrections are applied.

14. SUBJECT TERMS
Circulation Control, V/STOL Aircraft, Wind Tunnel Testing, Wing

15. NUMBER OF PAGES
73

16. PRICE CODE

17. SECURITY CLASSIFICATION OF REPORT	18. SECURITY CLASSIFICATION OF THIS PAGE	19. SECURITY CLASSIFICATION OF ABSTRACT	20. LIMITATION OF ABSTRACT
Unclassified	Unclassified	Unclassified	UL

NSN 7540-01-280-5500

GENERAL INSTRUCTIONS FOR COMPLETING SF 298

The Report Documentation Page (RDP) is used in announcing and cataloging reports. It is important that this information be consistent with the rest of the report, particularly the cover and title page. Instructions for filling in each block of the form follow. It is important to *stay within the lines* to meet *optical scanning requirements*.

Block 1. Agency Use Only *(Leave blank)*.

Block 2. Report Date. Full publication date including day, month, and year, if available (e.g. 1 Jan 88). Must cite at least the year.

Block 3. Type of Report and Dates Covered. State whether report is interim, final, etc. If applicable, enter inclusive report dates (e.g. 10 Jun 87 - 30 Jun 88).

Block 4. Title and Subtitle. A title is taken from the part of the report that provides the most meaningful and complete information. When a report is prepared in more than one volume, repeat the primary title, add volume number, and include subtitle for the specific volume. On classified documents enter the title classification in parentheses.

Block 5. Funding Numbers. To include contract and grant numbers; may include program element number(s), project number(s), task number(s), and work unit number(s). Use the following labels:

C	- Contract	PR	- Project
G	- Grant	TA	- Task
PE	- Program Element	WU	- Work Unit Accession No.

Block 6. Author(s). Name(s) of person(s) responsible for writing the report, performing the research, or credited with the content of the report. If editor or compiler, this should follow the name(s).

Block 7. Performing Organization Name(s) and Address(es). Self-explanatory

Block 8. Performing Organization Report Number. Enter the unique alphanumeric report number(s) assigned by the organization performing the report.

Block 9. Sponsoring/Monitoring Agency Name(s) and Address(es). Self-explanatory.

Block 10. Sponsoring/Monitoring Agency Report Number. *(If known)*

Block 11. Supplementary Notes. Enter information not included elsewhere such as: Prepared in cooperation with ; Trans. of , To be published in... When a report is revised, include a statement whether the new report supersedes or supplements the older report.

Block 12a. Distribution/Availability Statement. Denotes public availability or limitations. Cite any availability to the public. Enter additional limitations or special markings in all capitals (e.g. NOFORN, REL, ITAR).

> DOD - See DoDD 5230.24, "Distribution Statements on Technical Documents."
> DOE - See authorities.
> NASA - See Handbook NHB 2200.2.
> NTIS - Leave blank.

Block 12b. Distribution Code.

> DOD - Leave blank.
> DOE - Enter DOE distribution categories from the Standard Distribution for Unclassified Scientific and Technical Reports.
> NASA - Leave blank.
> NTIS - Leave blank.

Block 13. Abstract. Include a brief *(Maximum 200 words)* factual summary of the most significant information contained in the report.

Block 14. Subject Terms. Keywords or phrases identifying major subjects in the report.

Block 15. Number of Pages Enter the total number of pages.

Block 16. Price Code. Enter appropriate price code *(NTIS only)*.

Blocks 17. - 19. Security Classifications. Self-explanatory. Enter U.S. Security Classification in accordance with U.S. Security Regulations (i.e., UNCLASSIFIED). If form contains classified information, stamp classification on the top and bottom of the page.

Block 20. Limitation of Abstract. This block must be completed to assign a limitation to the abstract. Enter either UL (unlimited) or SAR (same as report). An entry in this block is necessary if the abstract is to be limited. If blank, the abstract is assumed to be unlimited.